




Predictive modelling of flow-accelerated corrosion – unresolved problems and issues

Authors Iva Betova, Martin Bojinov, Timo Saario

Confidentiality Public

Report's title Predictive modelling of flow-accelerated corrosion – unresolved problems and issues		
Customer, contact person, address SAFIR2010 / TEM	Order reference	
Project name Vesikemia ja hapettuminen reaktoripiirin olosuhteissa	Project number/Short name 41745 / WATCHEM	
Author(s) Iva Betova, Martin Bojinov, Timo Saario	Pages 53/	
Keywords flow accelerated corrosion, predictive modelling, commercial software codes, corrosion mechanism, hydrodynamical and mechanical factors	Report identification code VTT-R-08125-10	
<p>Summary</p> <p>Flow-Accelerated Corrosion (FAC) of carbon steel occurs due to the dissolution of the protective film that is formed on the surface and directly contacted with water. FAC is a practical threat to carbon steel piping within Nuclear Power Plant (NPP) steam cycle systems. Without a systematic pipe management program, rupture or leakage of piping or pipe components due to wall thickness reduction caused by FAC is inevitable. Pipe management program consists of several technical items, such as performing FAC model analyses, prioritizing pipe components for inspection, obtaining reliable thickness data, calculating the wear and wear rate, and making decisions regarding replacement necessity or continuous service acceptability based on the remaining life of the component.</p> <p>In the present literature review, the main emphasis is put on the predictive modelling of FAC including fundamental approaches such as the model of Sanchez-Calder and that of Lu and Luo, commercially available FAC rate prediction codes such as EPRI CHECWORKS, EdF BRT CICERO, KWU/AREVA WATHEC/COMSY, Russian codes such as RAMEK and ECI, as well as complex management programs including proposal and validation of FAC countermeasures using both laboratory and in-plant operational data (coupling analysis of corrosion and fluid dynamics, local flow approaches to two-phase flow accelerated corrosion, combinations between predictive modelling and monitoring etc.). The strengths and weaknesses of all the approaches are compared. In the Discussion section, the unresolved problems and issues related to both the corrosion mechanism itself and the proper definition of hydrodynamic and mechanical factors is outlined.</p>		
Confidentiality	Public	
Espoo 13.10.2010		
Signatures		
		
Timo Saario Chief Research Scientist	Petri Kinnunen Team Manager	Pentti Kauppinen Technology Manager
VTT's contact address P.O. Box 1000, FI-02044 VTT, Finland		
Distribution (customer and VTT) Customer 1, VTT 1		
<p><i>The use of the name of the Technical Research Centre of Finland (VTT) in advertising or publication in part of this report is only permissible with written authorisation from the Technical Research Centre of Finland.</i></p>		

Preface

Espoo 19.10.2010

Authors

Contents

1	Introduction	4
2	Goal	6
3	Description	6
4	Basic modelling of the FAC phenomenon	7
4.1	Sanchez-Caldera model	7
4.2	Mechano-electrochemical model of erosion-corrosion	9
5	Detailed modelling of FAC and associated predictive codes	11
5.1	KWU WATHEC / AREVA COMSY code	11
5.2	EdF CICERO code	15
5.3	Coupling analysis of corrosion and fluid dynamics (CAC-FD)	23
5.4	Local flow approaches to the two-phase flow-accelerated corrosion	29
5.5	Combination between calculation codes and monitoring	31
5.6	Approaches to FAC modelling in PHWRs	34
5.7	Prediction of FAC rates using the Russian codes RAMEK and ECI	37
6	Discussion	43
6.1	Modelling of the corrosion process and the influence of the oxide layer	43
6.1.1	Thermodynamic aspect (oxide solubility)	43
6.1.2	Kinetic aspect (growth and dissolution rates of the oxide)	46
6.2	Hydrodynamics, mechanical effects, and boundary layer thickness	48
7	Conclusions	50
8	Summary	50

1 Introduction

Flow-accelerated corrosion (FAC), also denoted as erosion-corrosion, of carbon or low-alloyed steel piping occurs when the rate of dissolution of the protective oxide film that forms on the internal piping surface into a stream of flowing water or wet steam is enhanced, leading to an increased wall thinning rate [1-4]. In general, the FAC process consists of two steps: the first step is the production of soluble iron at the oxide/water interface, while the second step is the transfer of the soluble and particulate corrosion products to the bulk flow across the diffusion boundary layer. Although FAC is characterized by a general reduction in pipe wall thickness for a given component, it frequently occurs over a limited area within this component due to the local high area of turbulence.

The rate of the wall metal loss due to FAC depends on a complex interaction of a number of parameters such as material composition, water chemistry, and hydrodynamics. The hydrodynamic parameters affect the mass transfer rate of the corrosion products to the bulk fluid and consequently the FAC rate. These hydrodynamic parameters are the flow velocity, pipe roughness, piping geometry, steam quality or void fraction for two-phase flows. Repeated inspections of power plants around the world have shown that piping components located downstream of flow singularities, such as sudden expansion/contractions, orifices, valves and elbows are most susceptible to FAC. This is attributed to the severe changes in flow direction as well as the development of secondary flow instabilities downstream of such singularities.

Several parameters influence the extent of degradation due to FAC, including the geometrical configuration of the components, piping orientation, flow Reynolds number, fluid chemistry, fluid temperature, piping material and the flow turbulence structure which affect the surface shear stress and mass transfer coefficients. An early review of FAC in power plants piping systems has been published by Poulson [3]. He noted that the single and two-phase flow conditions result in two very different wear patterns. More recently, Schmitt and Bakalli [5] suggested that FAC is initiated when the flow dynamic forces surpass the fracture energy of the protective layers.

This brings up the question of the interaction between mechanical and electrochemical factors during erosion-corrosion. In line with the mechanisms of material removal during such processes [6,7], the total material loss W_t , can be expressed as the sum of the corrosion component W_c and the erosion component W_e :

$$W_t = W_c + W_e \quad (1)$$

Since the corrosion is dominated by electrochemical reactions, the material loss due to corrosion can be related to the dissolution current density i_d via Faraday's law

$$W_c = M \frac{i_a}{nF} = W_F \quad (2)$$

The erosion component of the material loss results from the action of various mechanical forces on the surface of the components. During this process the material is removed and normally enters the solutions before being ionized, in the form of debris or chipping. Therefore, the wall thinning due to erosion process can be regarded as non-Faraday material loss, in other words

$$W_t = W_F + W_{n-F} \quad (3)$$

Due to the interaction between the mechanical and electrochemical damage processes, erosion and corrosion can actually enhance each other [6,7]. Thus, compared with the situation in which erosion or corrosion occur separately, additional material losses have to be included in both of the Faraday component and the non-Faraday component

$$W_F = W_{c,0} + W_{e-c}, \quad W_{n-F} = W_{e,0} + W_{c-e} \quad (4)$$

where $W_{c,0}$ and $W_{e,0}$ are the material losses due to corrosion and erosion alone.

In fact, the dissolution current density mentioned above (equation (2)) is equal to the sum of the current densities of the dissolution of the oxide and transfer of iron ions from the metal through the oxide layer, which emphasizes the role of this layer as one of the controlling factors of FAC [8,9]. Several works [8-11] have been devoted to the characterization of the thin iron oxide layers formed on the carbon steel components under the chemical and hydrodynamical conditions prevailing within the secondary circuit of PWR plants (deaerated and alkaline turbulent water or wet steam). Using a range of techniques such as low-energy electron induced X-ray spectrometry (LEEKS), X-ray diffraction (XRD), scanning electron microscopy (SEM), Auger electron spectroscopy (AES), glow-discharge optical spectrometry (GDOES) and atomic force microscopy (AFM) has allowed to get information on the nature, thickness and structure of the surface oxide layer and to put in light the influence of the alkaline reducing agents (e.g. hydrazine) added to the feedwater. It has been shown that the oxide with a thickness of 500-700 nm has a bilayer structure and consists largely of magnetite-type phase with some oxidized Ni incorporated in it, although other experimental results from Fourier-transform Infrared Spectroscopy (FT-IR) pointed to the formation of the maghemite phase as well.

A summary of the processes involved in the FAC phenomenon according to this short introduction is presented in Figure 1.

For the identification of system areas which are sensitive to flow-induced corrosion and associated types of degradation (droplet impingement erosion, corrosion cavitation), a comprehensive plant-wide strategy needs to be applied. This needs to incorporate predictive software functionalities which enable the identification of plant areas susceptible to wall thinning based on system parameters in combination with material data. If a system area is identified as being susceptible to FAC, a detailed analysis of the respective system area needs to be initiated. Based on a predictive code evaluation, the inspection program can be optimized by focusing activities on degradation sensitive areas. The integrated inspection data management function is expected to ensure information feedback,

i.e. the predictions are calibrated against the inspection results. Such a strategy is assumed to provide a comprehensive, long-term surveillance of the integrity of mechanical components.

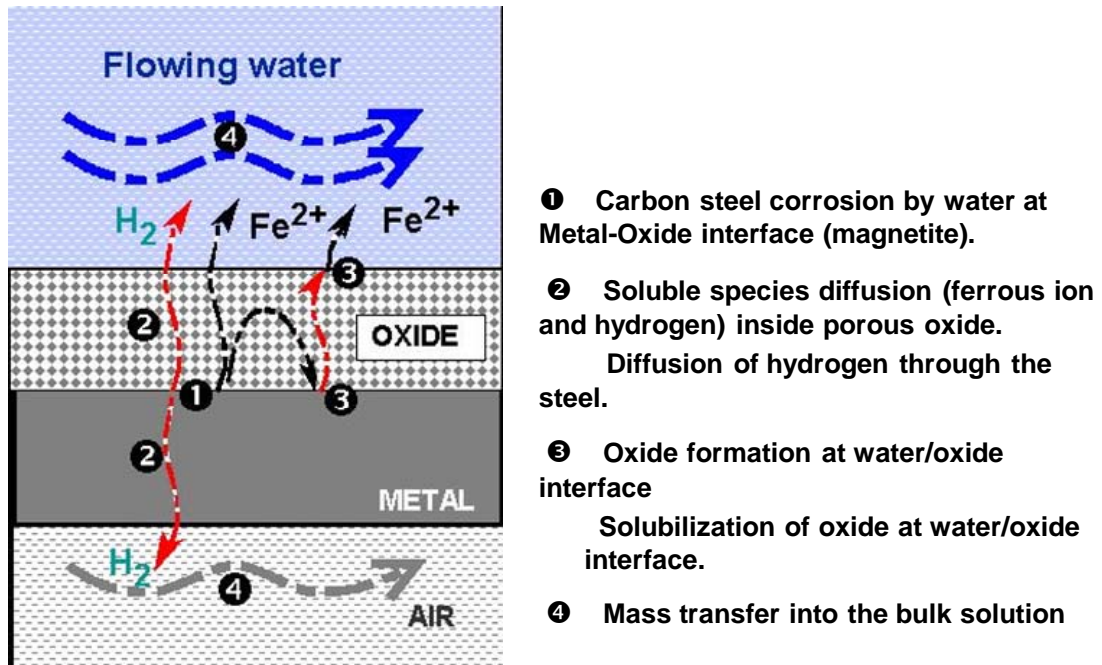


Figure 1 Summary of the processes involved in the FAC phenomenon.

2 Goal

The main goal of the present survey is to review the existing models, associated software prediction tools and FAC management strategies for water-steam cycle power plants. Although naturally main emphasis is placed on nuclear power plants for which the major part of secondary side piping accidents have been reported and thoroughly analysed, the systematic overview of the available information will be of use to fossil power plants and other compatible industrial installations as well.

3 Description

In the following, first the fundamental models that attempt to explain the interplay between corrosion, hydrodynamics, material properties and mechanical factors will be presented that have served as a basis to the understanding of FAC. Second, the main software prediction tools that are both commercially available or under development are described in detail, the emphasis being put on the physico-chemical, mechanical and mathematical models underlying the respective software rather than a comprehensive comparison of their predictive abilities. Finally, in a Discussion section, the unsolved problems in this particular area of scientific endeavour and industrial enterprise are pointed out and directions for further research – both from the experimental and modelling point of view – are given.

4 Basic modeling of the FAC phenomenon

4.1 Sanchez-Caldera model

The removal of material by corrosive-erosive wear is a result of several phenomena, including the initial reaction of pure iron with water and the final step of mass transport of hydroxides into the bulk flow of water. The oxide layer formed on iron plays an important role by restricting the flow of water to the metal and the flow of hydroxides by diffusion from the iron surface to the water flow; those factors in turn affect the hydroxide concentration at the iron-oxide and oxide-water interfaces [12]. The process of corrosion-erosion includes complicated chemical kinetics and fluid mechanics. It is difficult to incorporate all the process laws in the derivation of the model; instead, Sanchez-Caldera et al. looked for the minimum number of variables necessary to explain the experimental data [12]. The experimental data indicated that: (a) the wear is a linear function of time; (b) the wear rate is maximum at a temperature near 150 °C and (c) the wear increases with fluid velocity. With the above ideas, the following equation was derived:

$$\frac{dm}{dt} = \frac{\theta(c_e - c_\infty)}{(1/k) + (1-f)[(1/K_d) + (d/D)]} \quad (5)$$

where dm/dt is wall thinning rate in $\text{mol cm}^{-2}\text{s}^{-1}$ (to be determined); c_e – equilibrium concentration of iron species (in mol cm^{-3}), which depends on temperature, hydrogen concentration, and pH; θ – porosity in cm^2 of open area/ cm^2 of metal or $\text{cm}^{-3} \text{H}_2\text{O}/\text{cm}^3$; K_d – mass transfer coefficient in cm s^{-1} ; $k = A \exp(-E/RT)$, the reaction rate constant in cm s^{-1} ; f – fraction of oxidized metal converted into magnetite at the metal-oxide interface, d – magnetite thickness in cm, D – diffusion coefficient of iron cations in water, c_∞ – iron species concentration in the bulk fluid, mol cm^{-3} .

The assumptions made by the authors to derive equation (5) have been the following [12]:

- (1) A steady state is considered. The oxide layer has been developed, and its thickness (d) and porosity (θ) have attained a constant value as a function of time.
- (2) Of the amount of iron oxidized at the metal-oxide interface, a fraction f is converted into magnetite; this is the same amount being removed at the oxide-water interface. It has been assumed that f has a fixed value of 0.5. This value is based on static experiments of the corrosion of steel; where, in general, a bilayer oxide is formed and the outer oxide layer has the same amount of iron as the inner layer.
- (3) There is no net circulation or flow of water inside the oxide; therefore, the simulation of the transport of species inside the layer can be considered as a concentration diffusion problem.
- (4) The water contains low concentrations of oxygen (<200 ppb), and the only oxide present is magnetite.
- (5) The reaction at the metal-oxide interface proceeds at a rate equal to

$$\frac{dm}{dt} = k\theta(c_e - c_0) \quad (6)$$

where k is equal to $A \exp(-E/RT)$. This implies that the reaction rate at the metal surface is proportional to the potential created by the concentration difference between c_e , the equilibrium concentration of hydroxides (their solubility), and c_0 , the actual concentration of hydroxides at the metal-oxide interface.

(6) The hydroxides diffuse through the pores in the oxide due to differences in concentration from the metal to the water. The diffusion path length is considered to be equal to the oxide thickness,

$$(1-f) \frac{dm}{dt} = \frac{D\theta}{d}(c_0 - c_1) \quad (7)$$

(7) At the oxide-water interface, the concentration at the pores is c_1 , but everywhere else it is different. The mass transfer rate from the pores to the water is considered to be equal to $h_d\theta(c_1 - c_\infty)$, and the mass transfer rate from the nonporous oxide is equal to the rate of magnetite formed at the metal-oxide interface.

The above assumption permits the use of the following equations to represent the wear rate dm/dt [12]:

$$\begin{aligned} \frac{dm}{dt} &= k\theta(c_e - c_0) \text{ (see assumption 5)} \\ (1-f) \frac{dm}{dt} &= \frac{D\theta}{d}(c_0 - c_1) \text{ (see assumption 6)} \\ (1-f) \frac{dm}{dt} &= K_d\theta(c_1 - c_\infty) \text{ (see assumption 7)} \end{aligned} \quad (8)$$

This system of three equations with three unknowns dm/dt , C_1 , and C_0 , can be solved for dm/dt , yielding equation (5).

The model has been subjected to initial validation with experimental data [12]. The study has shown that the most important assumptions made. i.e., a constant wear rate, and a reaction rate constant following an Arrhenius function with temperature, have been proven appropriate. The values of the parameters used for K_d , D , d , and θ were verified and calculated by different relations. An additional hypothesis of the authors is that at higher temperatures, the faster chemical reactions lead to a decrease in porosity. The complete model therefore takes the following form:

$$\frac{dm}{dt} = \frac{\theta(c_e - c_0)}{(1/k) + (1-f)[1/K_d + d/D]} \quad (9)$$

where $k = 2.35E14 \exp(-35.380/RT)$ in SI units, and $\theta = 0.05$ at $T < 422$ °F (300 °C) or $\theta = 6.75 \cdot 10^{-3} - 1.48 \cdot 10^{-5} T(K)$, for $422 < T < 449$ °F. Using eq. (9), a procedure to estimate the wall thinning rate has been developed, and agreement between experimental and theoretical values has been found to be good. Specifically, at high fluid velocities, the calculated values were found to be within 30 percent of the experimental data.

Summarising, the Sanchez-Caldera model has the advantages of being rather simple yet encompasses several of the most important factors influencing FAC. This is why it has been widely used as a basis for software prediction tools of the wall thinning rates due to FAC. However, the model does not take into account the bilayer structure of the oxide film, as well as the possibility of an alteration of the mechanical and electrochemical properties of the surface layer at the oxide/electrolyte interface. A more thorough discussion on possible improvements in the Sanchez-Caldera model is given in the Discussion section of the present survey.

4.2 Mechano-electrochemical model of erosion-corrosion

A theoretical model of the interaction between electrochemical and mechanical factors during erosion-corrosion [7,13] has been developed on basis of nonequilibrium thermodynamics, dislocation kinetics, and electrochemistry. The model has been presumed to lead to the quantitative assessment of material loss produced by the synergism of mechanical and electrochemical factors in an erosion-corrosion process. The fundamentals of the model are briefly discussed below.

As corrosion-induced erosion occurs on the sample surface, it can be expected that the weight loss involved, W_{c-e} (see eqn. (4)) can be related to the material intrinsic properties $\phi_1(m)$, the mechanical forces related to hydrodynamic parameters $\phi_2(f)$, and the properties of the surface oxide layer $\phi_3(s)$

$$W_{c-e} = \phi_1(m)\phi_2(f)\phi_3(s) \quad (10)$$

According to the model, the intrinsic properties of the material depend mainly on the interatomic bonding which determines the resistance of the atoms to be removed by external force. Thus, different material may show different corrosion-induced erosion rate in same environment. For the second term, the hydrodynamic pattern of corrosive media represents the intensity of the external force exerted on the material surface. Finally, the third term $\phi_3(s)$ comes from the mechanical properties of surface layers, which could be influenced by some processes, such as the corrosion reaction.

According to the proposed approach, the corrosion-enhanced erosion in slurry results from the dissolution-induced hardness degradation of the surface layer. This hardness degradation can be formulated by:

$$\frac{\Delta H_v}{H_{v_0}} = -B \log \frac{i_a}{i_{th}} \quad (11)$$

where $\Delta H_v = H_v - H_{v_0}$ is the change in hardness due to dissolution at the surface, H_v is the hardness with the presence of anodic current at the electrode surface, $B (>0)$ is an experimental constant, and i_{th} is the threshold dissolution current density to induce the hardness degradation of the surface layer.

Experimental results of the authors [7] have indicated that the corrosion-induced erosion disappears when the sample is under cathodic protection, i.e. when

corrosion rate is substantially decreased no hardness degradation occurs. Conversely, corrosion-induced erosion is enhanced by an increase in the dissolution current density or by a decrease in hardness. Based on these observations, the authors proposed the following equation for the surface layer degradation term in eq. (10)

$$\phi_3(s) = k'(-\Delta Hv)^m \quad (12)$$

For carbon steel with moderate hardness, $m=1$ [6], i.e. at constant hydrodynamic conditions

$$W_{c-e} \approx -K\Delta Hv, K = k'\phi_1(m)\phi_2(f) \quad (13)$$

Further, inserting eq. (11) in (13) and grouping the constants, the authors arrive at

$$W_{c-e} = A \log \frac{i_a}{i_{th}}, A = KBHv_0 \quad (14)$$

As predicted by this model, the synergistic effect results mainly from the interaction of two irreversible fluxes, namely, the dissolution current density and the plastic flow in the surface layer caused by dynamic plastic deformation. Meanwhile, the dissolution current at the wall surface, in turn, can increase the mobility of dislocations and reduce the resistance in the surface layer against plastic deformation (Figure 2). Such an effect has been demonstrated by the hardness degradation of metals in corrosive media. The degradation of mechanical erosion resistance with decreasing hardness suggests that the corrosion-enhanced erosion may result from the degradation in hardness of target material induced by the anodic dissolution and the corresponding wastage is also a linear function of the logarithm of anodic current density.

It can be concluded that while the model of Lu and Luo captures several interactions between mechanical and electrochemical factors in erosion-corrosion, further work especially on the hydrodynamic correlations, as well as the material correlations is needed in order to transform this model into a predictive tool for wall thinning rates of piping in power plants.

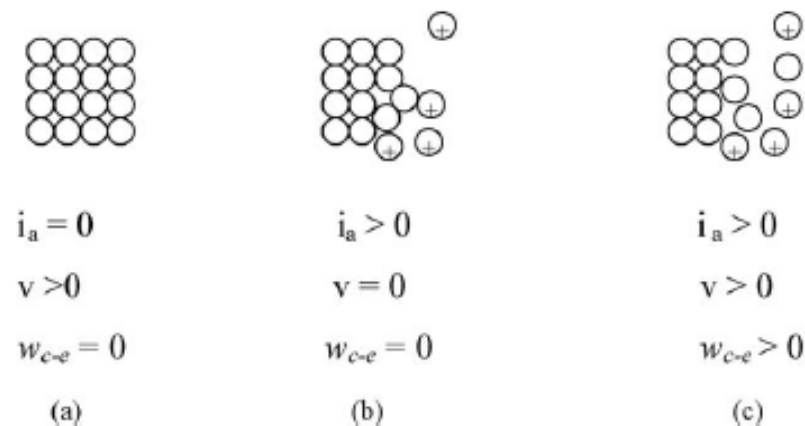


Figure 2 Corrosion-induced erosion in different cases according to the mechano-electrochemical model of Lu and Luo [7,13]: a) under cathodic protection, (b) in stagnant solution and c) in flowing solution.

5 Detailed modelling of FAC and associated predictive codes

5.1 KWU WATHEC / AREVA COMSY code

Due to the large number of factors influencing the degree of material loss due to erosion corrosion, the analysis of such damage is possible only with the aid of a computer code. Extensive experimental and theoretical investigations have been performed to develop a calculation code for wall thinning due to erosion corrosion in power piping systems. The so-called WATHEC code can be applied to single-phase water flow as well as to two-phase water/steam systems [14]. Only input data which are available to the design engineer or the operator of a plant are taken into consideration. The parameters affecting material loss from steel surfaces due to erosion corrosion were established in extensive laboratory experiments carried out by Siemens/KWU, as part of a research program. Kastner et al. [14] have shown that other important factors besides the geometry conditions, which are dealt with more closely in the following, are the material composition – principally the chromium and molybdenum and, also the copper content – and the flow velocity of the water. Of major impact are the temperature, pH and oxygen content of the water. In BWR plants, highly pure de-ionized water is used as the fluid of the steam-water cycle. It contains oxygen and has a pH close to neutral. The presence of an adequate amount of oxygen in the feedwater (optimum around 50 ppb) results in good water chemistry protection against erosion corrosion.

In most cases the fluid temperature is given, and water chemistry can be adjusted only within a limited range as dictated by other parameters. For this reason the following items are of great practical importance:

- Material selection: austenitic stainless steels are not susceptible to erosion corrosion; the resistance of carbon and low-alloy steels increases with chromium, molybdenum and copper content [14].
- Flow velocity: this can be limited for a given mass flow by selecting suitable line cross sections.
- Pipe geometry: this can be optimized to improve flow conditions by selecting sufficiently large elbow radii, replacing T-fittings with laterals, etc.

Laboratory experiments were carried out to develop an empirical relationship for the calculation of material loss due to erosion corrosion. This relationship was found to apply in the first instance to single-phase flow only. It could, however, following slight modification, be applied to two-phase flow, but only provided the metal wall is wetted by a continuously moving, coherent film of water [14]. The flow velocity in such a case has been taken to be the mean velocity of the water film along the pipe wall, which is dependent on the mass flow rate, on the density of the water under saturation conditions, on the steam quality and the void fraction. At the same time, the pH and oxygen content parameters input into the calculation have taken into account the temperature- and pressure-dependent distribution coefficients for alkalizing agents and for oxygen.

As prediction accuracy has been found to depend significantly on the quality of the input data, the model has been tested extensively and calibrated to plant data in order to ensure conservative prediction on the one hand and to avoid

overestimation of in-plant erosion corrosion material losses on the other. These requirements were taken into account during development of the WATHEC code by comparing the calculated material losses with measured values taken from other laboratory experiments and with data gathered during power plant operation. These data are continuously stored in a database, set up and continuously updated by KWU and later AREVA.

In piping systems, components which disturb normal flow and thus create turbulence are often located only short distance apart. In such cases, the turbulence created by an upstream component A with geometry factor $k_{c,A}$ has not yet completely subsided when the water flowing in the pipe reaches component B with geometry factor $k_{c,B}$. For reliable and conservative prediction of erosion corrosion material loss a portion of $k_{c,A}$ must thus be taken into account in determining the geometry factor for component B.

The portion of the geometry factor from component A remaining can be described by means of an exponential function [14]:

$$\Delta k_{c,A} = k_{c,A} \exp(-Cz / D_p) \quad (15)$$

where D_p is pipe diameter, z the distance from component A, and C is a constant ($=0.231$). The validity of this relation has been demonstrated by the following examples: material loss due to erosion-corrosion on a test setup consisting of a sharp elbow followed by straight piping of the same diameter was investigated in a laboratory experiment. It has been found that wall thinning due to erosion corrosion enlarges the pipe diameter. The decrease in material loss due to erosion corrosion in the region $0 \leq z / D_p \leq 10$ shows essentially the pattern predicted by eq. (15) for the respective geometry factors. The geometry factor for a component B a short distance downstream of component A has been calculated using the following equation:

$$(k_{c,B}) = k_{c,B} + (k_{c,A}) \quad (16)$$

It has to be borne in mind that the geometry factor for a combination of components cannot exceed the value for stagnation point flow

$$(k_{c,B})_{tot} \leq 1.0 \quad (17)$$

The considerations presented here relate to a single-phase flow in which the extent of turbulent effects is limited to $z = 10D_p$. In a two-phase (steam/water) flow this extent might be much larger, depending on the steam quality. The presentation of material loss over the length of the piping system also included the local (obtained by wall thickness measurement) and average (by weighing) material losses determined as part of the experiment. In addition to a quite good agreement between calculated and measured values, the comparison also showed that the computer code is adequately capable of calculating the flow disturbances caused by turbulence-inducing components.

Weak point analysis The WATHEC program was developed for the determination of the material removal to be expected in a power plant component or a piping

system and/or to predict the remaining life expectancy of a component under the given loading conditions [13]. This application is best pursued as part of a "weak point analysis", the sequence of which is as follows. On the basis of operational data, plant systems, which lie within the crucial range of relevant parameters within which erosion corrosion on a significant scale is possible at all, are first selected. Within these systems, the points most susceptible to damage are identified on the basis of the pertaining geometry and flow conditions. The material loss to be expected at these potentially weak points is then calculated with the aid of the prediction model. The results of these calculations are subjected to a critical analysis including, for instance, an appraisal on the basis of the measurement data available in the data base.

The prediction model has been found to be of broader benefit for two reasons: in plants in which the crucial aspects identified have been fully taken into account, for instance in terms of flow conditions or of pH levels, the model could give indications of the current component condition. In addition, application of the model has been demonstrated to be particularly important when a thought is being given to reducing measurement and monitoring effort and to extending the life expectancy of components of whole piping systems.

Further model development Based on the experimental investigations performed at AREVA test facilities an empirical calculation model was developed in the late 1970s. The model was further improved and integrated with the PC code WATHEC for performing analysis for piping systems in respect to flow-accelerated material degradation. In addition, the PC program DASY was applied for recording, managing, evaluating and documenting the data obtained from nondestructive examination (NDE) of individual piping components. In 1998 the FAC-model was further developed to produce the COMSY software system as an integrated tool for ageing and plant life management of mechanical components.

Strategy applied for the degradation analysis In order to efficiently screen a plant unit for systems or components potentially affected by FAC, operating and design data have to be systematically assessed on a cross-system basis. The evaluation of the degradation potential for plant system requires key parameters for the following items:

- Operational conditions (e.g. temperature, pressure, flow condition, steam quality)
- Water chemistry conditions (e.g. pH value, oxygen concentration)
- Material properties (e.g. alloy content, allowable stress, yield stress).

In the next step key parameters for individual system areas are compared with parameter ranges relevant for the occurrence of FAC, in order to determine for which power plant systems a degradation potential exists.

During the screening process the heat balance diagram of the water/ steam cycle in the power plant is modeled using graphical tools. Further on system parameters (mass flow, pressure, temperature, steam quality etc.) are specified for each section. In addition, injection positions for the water chemical treatment are defined by the type (concentration of alkalizing agents and/or oxygen concentration). The resulting model [15] establishes the basic structure of the virtual power plant and allows an analysis of the water chemistry cycle to be performed based on the thermohydraulic parameters. Taking into consideration

the material properties used in each case (e.g. alloy contents, allowable stress), the sections are then assessed in respect to degradation potential imposed by FAC. In system areas in which the occurrence of a specific degradation mechanism is possible, the existing sensitivity should be analyzed within the scope of a detailed analysis. This second step, which is based on the information used for the performance of the screening study, requires more detailed information on the relevant systems or components. Additional information, such as e.g. the geometrical configuration of piping systems, is also needed for determining the local fluid dynamic parameters required for degradation rate prediction. The detailed analysis procedure results in an automatic generation of service life predictions for each component.

The lifetime prediction chart (Figure 3) shows the conservatively predicted wall thinning (red line) and the calibrated wall thinning (blue line) versus the operation time of the component [15]. The colored ranges indicate piping integrity criteria (manufacturing tolerance, minimum wall thickness, yield stress condition and tensile stress condition). The green color tolerance bar indicates the wall thickness examination result, e.g. performed in 2003. Based on the evaluation in respect to degradation potential and remaining lifetime, components are prioritized for examination programs and condition-oriented inspection plans are generated.

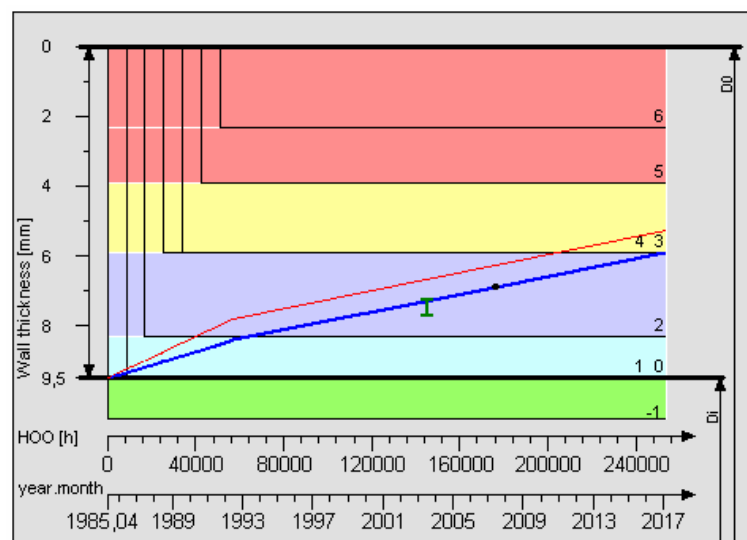


Figure 3. Lifetime prediction chart of the COMSY code.

Risk-based selection of examination locations [15,16] Both the probability of occurrence of degradation as well as the safety risk or economic consequences of potential degradation must be accounted for in the selection of examination locations. Safety classes or availability categories are specified for the individual system areas. The program uses these to calculate the consequences of degradation, which serves as the ordinate of the cluster diagram (Figure 4).

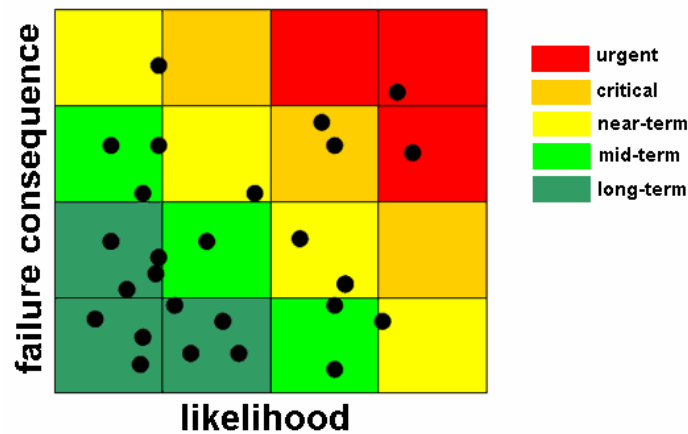


Figure 4. Risk matrix of the COMSY code.

The probability of degradation for the mechanisms under consideration is plotted on the abscissa. The specific selection of locations for inspection is performed interactively in a ranking table. A suitable examination method is also proposed for each relevant degradation mechanism.

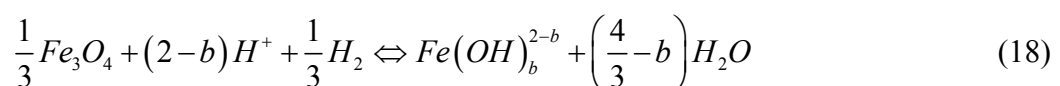
Evaluation of examination results [15,16] The COMSY software system acquires and evaluates data from nondestructive component examinations (weld examination, wall thickness examination, ultrasonic examination, visual inspections etc.). The examination results are recorded in standardized formats and are assigned to the examined component for documentation of the actual condition for the corresponding point in time in the operating history of the plant and integrated in the virtual power plant data model.

5.2 EdF CICERO code

According to the early EdF views [17], flow-assisted corrosion has been regarded as a completely deterministic phenomenon. It concerns the carbon steel equipment where hot degassed water flows. The influence of several parameters: on one hand, the redox equilibrium fixed by the ferrous iron ion concentration; on the other hand, convective diffusion transport of soluble products into the flow [17] is explained through an analytical model. A means of estimating quantitatively the corrosion kinetics in terms of wall thinning is given. Both single- and two-phase flows are considered.

The first step of the process, as usual, concerns the production of soluble ferrous ions [17]:

- Metal oxidation at the iron-magnetite interface and diffusion of resulting ferrous ions from the iron surface to the main water flow through the oxide layer. It can be assumed, based on e.g. the volume difference between the metal and magnetite (a factor of about two) that roughly half of the metal ions form the oxide and the rest form the ferrous ion diffusion flow.
- Reductive dissolution of the magnetite layer at the oxide-water interface that is expected to be in equilibrium:



where $b = 0,1,2,3$ and 4. The ferrous ion production is a steady state corrosion process exhibiting linear corrosion kinetics; the reduced magnetite layer at the oxide/water interface is replaced by a new magnetite layer of the same thickness at the metal/oxide interface. The rate of dissolution at the external surface of the magnetite can be written as a first-order reaction

$$V_{c,Fe_3O_4diss} = k(c_{eq} - c) \quad (19)$$

where k is the reaction rate constant, c_{eq} the soluble ferrous ion concentration at equilibrium with the magnetite, and c the soluble ion concentration at the oxide-water interface. The formation of ferrous ions via reductive dissolution at the oxide/water interface represents a part of the total ferrous ions production. The authors have assumed that this part forms half of the total production [17], resulting in a total corrosion rate expressed as

$$V_C = 2k(c_{eq} - c) \quad (20)$$

The value of c_{eq} depends on the pH of the water, the hydrogen pressure P_{H_2} and the temperature.

The second step is related to the transfer of the ferrous ions in the bulk water. The ferrous ion flux F_{IF} can be modeled as a convective transport phenomenon:

$$F_{IF} = K_d(c - c_\infty) \quad (21)$$

where K_d is the mass transfer coefficient and c_∞ the ferrous ion concentration in the bulk of the fluid. When both steps have become stationary, F_{IF} and V_C are equal, i.e. $2k(c_{eq} - c) = K_d(c - c_\infty)$. Solving for c and inserting in eq. (20) one can associate the soluble-iron species production and the mass transfer effect on erosion-corrosion in the general equation:

$$V_C = 2K_d k(c_{eq} - c_\infty) / (K_d + 2k) \quad (22)$$

The main results obtained in a single-phase or two-phase flows showed, in deoxygenated and alkaline water, and if c_∞ is near to zero, that the erosion-corrosion rate is proportional to c_{eq} and to K_d . In fact the reaction kinetic is faster than the mass transfer ($k \gg K_d$): the erosion-corrosion is a convective diffusion-controlled process [17]. The relation between the mass flux, the mass transfer coefficient and the ferrous iron concentration at the equilibrium becomes:

$$V_C = K_d c_{eq} \quad (23)$$

If c_{eq} is the volumetric concentration (iron volume into water volume), eq. (23) gives the thickness loss kinetics T_L :

$$T_L = K_d c_{eq} \quad (24)$$

According to the EdF approach, each parameter that governs FAC intervenes through the mass transfer coefficient and the ferrous iron concentration.

Effect of pH The general corrosion behaviour of carbon steel in water can be predicted using potential – pH diagrams (Figure 5). In high-temperature deoxygenated water, the potential of carbon steels is close to that corresponding to the hydrogen evolution reaction:

- In alkaline water a thermodynamically stable film of magnetite (Fe_3O_4) is formed over a wide range of pH values, including the cold pH range 8.5 – 10 typical of the PWR secondary circuit (Figure 5). Under these conditions, erosion-corrosion is not independent of the alkalinizing agent; the critical parameter is the hot pH or the ferrous iron concentration at the equilibrium. In a two-phase flow, the steam quality and the steam-water partition of the alkalinizing agent must be considered.
- In the absence of water treatment, as met in BWR where pure water is used, the ferrous ion Fe^{2+} is thermodynamically stable, instead of magnetite. In this case, the basic model can also be applicable. The pH value to take into account is the local pH at the steel surface.

Influence of oxygen content Experiments showed that the oxygen effect depends on the mass transfer coefficient [17]. There is a threshold value, which can be understood from a potential-pH diagram (Figure 5): when the oxygen level increases, the characteristic point moves to a higher potential and hematite is formed instead of magnetite. Because the solubility of hematite is much less than that of magnetite, the oxide film is presumed to be much more resistant to erosion-corrosion. The results obtained in a loop at 180 °C with the oxygen level monitored between 0 to 15 ppb showed a very low sensitivity for oxygen content between 0 and 7 ppb, but for all temperatures a 15 ppb concentration is probably over the threshold. In a two-phase flow, no oxygen effect would be expected, as long as the humidity is enough to assure a water film at the wall. Following the Dalton law, the oxygen in a saturated stream-water mixture is completely located in the steam if the partial pressure of the oxygen is less than that corresponding to 100 ppb.

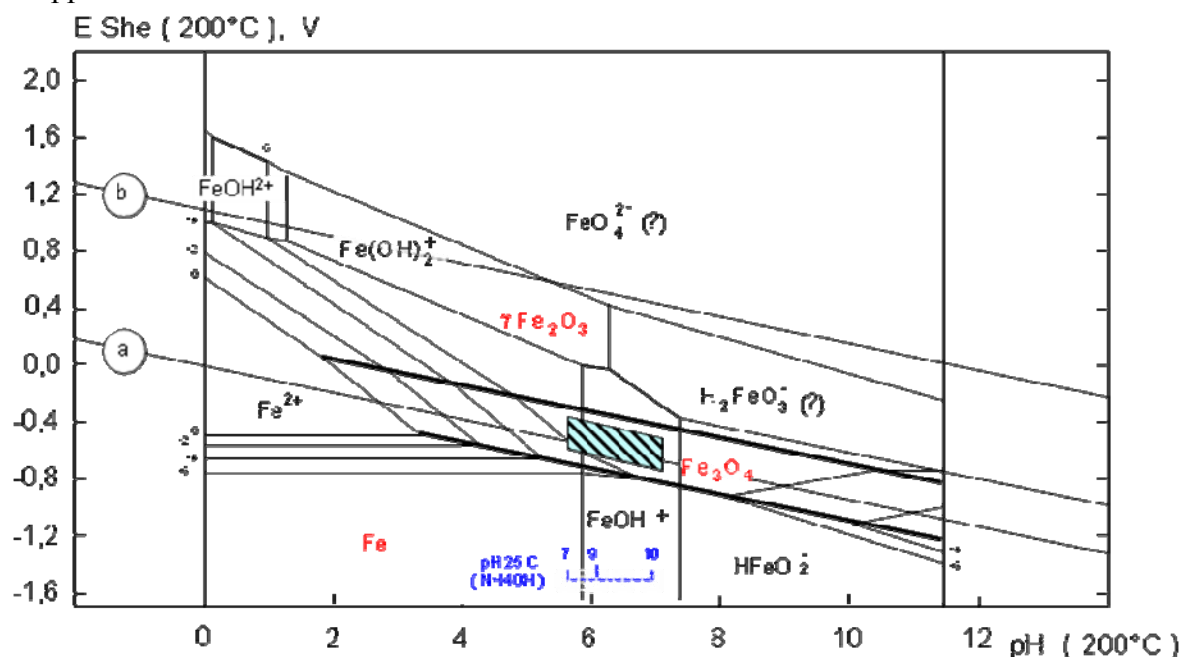


Figure 5 Potential – pH diagram of the system $\text{Fe-H}_2\text{O}$ at 200 °C and the FAC zone.

Influence of temperature Temperature is a parameter the influence of which is not direct. On the one hand, when the temperature increases, the ferrous iron concentration decreases; that signifies that at low temperature, the capacity of water to remove ferrous iron is at a maximum. But, on the other hand, the temperature effect is very important on the flow viscosity and on the ferrous iron diffusivity, which governs the mass transfer. This explains why the position of the maximum on published curves [17] depends clearly upon the test conditions.

Effect of steel composition Several authors have reported that the addition of chromium has a beneficial effect on the resistance to erosion-corrosion [18]. A systematic study has been made on low-alloyed steels. The effect of the actual chemical composition of the steels can be written as

$$T_{LA} = T_L f(Cr, Mo, Cu) \quad (25)$$

The last function was [17] explicitated as

$$F((Cr), (Mo), (Cu)) = B / ((Cr)^{0.89} (Mo)^{0.2} (Cu)^{0.25}) \quad (26)$$

where (Cr), (Mo) and (Cu) are the concentrations expressed in percent. This relation has been verified even for very low concentrations and for pure iron. The value of B is given by the threshold under which the impurities do not influence the wear kinetics.

Influence of the mass transfer – mass transfer is the second key parameter for the understanding of the erosion-corrosion mechanism. The characteristic mass transfer number is the Sherwood number, which is written as

$$Sh = K_d d / D \quad (27)$$

where d is the tube diameter or a characteristic geometric dimension and D the ferrous ion diffusion coefficient in water. In relation to FAC, a new adimensional criterion has been proposed, which characterised the thinning kinetics (W).

$$W = T_L d / DC_{eq} \quad (28)$$

Remy and Bouchacourt [17] considered the case of the straight tube, where the mass transfer could be easily evaluated by the Dittus-Boettler correlation. However, tests are carried out with a Reynolds number lower than 2×10^5 , and feedwater piping systems of power station are characterised by Reynolds number around 2×10^7 . The in situ measurements came from straight corroded pipes in a power plant where the thinning kinetics was large enough to observe wear on the straight part of the pipes. Temperature was between 180 and 225 °C and the value of the room temperature pH was equal to 8.8. In addition to the validation of the above assumption, two important conclusions could be drawn:

- The thinning is strictly proportional to time – both in laboratory tests up to 200 h and thickness loss after 60 000 h in operation.
- W is strictly equal to Sh . This point shows that the hydrogen concentration to be taken into account corresponds to a partial pressure equal to 1 bar at 25 °C.

Application for the prediction of thickness loss Erosion-corrosion appears at first in the piping singularities. In this case, there are not general correlations to deduce mass transfer from hydrodynamic conditions. To obtain mass transfer data in a general form, Remy and Bouchacourt [17] used the same correlation as in a straight tube, with an enhancement coefficient A depending on the type of

singularity. Strictly, in fact, if several partial correlations are considered, the exponent to be applied at the Reynolds number is varying between 0.6 and 0.8. In a practical Reynolds number range, this difference corresponds to an uncertainly range of $\pm 20\%$. For a two-phase flow, the mass transfer coefficient has been evaluated from a similar correlation, in which Re has been calculated with the actual water velocity taking into account the void fraction between steam and water. The value of the coefficient A is obtained from data for the thickness measurements performed on power units owned by EdF or other utilities, where small or large amounts of wear have occurred. The chromium content for each datum is estimated from a sample of 200 chromium content analyses. In the resulting database, Remy and Bouchacourt [17] have taken into account the following types of singularities: straight tubes, elbows, bifurcations, tube downstream regulating valves, diaphragms or divergent sections. For the elbows, the value of A has been found to depend on the angle and on the curvature of the elbow. The wear kinetics in a bifurcation has been assumed to depend on the ratio between the main to branch velocity and on the angle of the lateral pipe to the main. The thinning of a given singularity was larger if another singularity took place in the near upstream region. The authors proposed several correlations to take into account these supplementary parameters and use them in the wear prediction study. They have been derived from considerations of the similarity between the convective mechanism and the flow-wall friction, and were partly validated by in situ measurements.

As mentioned already above, EdF initially used a classical deterministic approach [19]. The algorithm for kinetics calculation has been derived from the Sanchez-Caldera model [6] described by equation (5). The model took into account all the parameters which have an effect on the intensity of the FAC phenomenon. The chemistry of water is taken into account through c_e , the content of soluble ferrous ion at equilibrium with magnetite at the oxide/water interface, and c_∞ , the content of soluble ferrous ion concentration in the bulk fluid. As already mentioned above, the value of c_e depends on the hydrogen pressure p_{H_2} , the hot pH and the equilibrium constants of various soluble ferro-iron species as calculated according to [6]:

$$c_e = (p_{H_2})^{1/3} \cdot [K_1 c_{H^+}^2 + K_2 c_{H^+} + K_3 + K_4 / c_{H^+}] \quad (29)$$

where K_1 , K_2 , K_3 and K_4 are the respective constants of equilibrium of the species Fe^{2+} , $Fe(OH)^+$, $Fe(OH)_2$ and $Fe(OH)_3^-$.

The thermohydraulic conditions of each pipe element are taken into account by the coefficient of mass transfer K_d that is equal to the coefficient of mass transfer of a straight tube of the same diameter k_{ST} multiplied by a geometry factor (Geo) according to the modified Colburn formulation:

$$K_d = Geo \times k_{ST} \quad (30)$$

with k_{ST} determined from the modified Colburn's relation and validation in a test loop called CIROCO.

$$k_{ST} = 0.0193 (D/d) (e/d)^{0.2} Re Sc^{0.4} \quad (31)$$

with:

e – roughness (in BRT-CICERO this value is set at 4×10^{-5} m), d – internal diameter (hydraulic diameter) of the component, Re – Reynolds number and Sc – Schmidt number.

To take into account the shape of the components, a geometry factor is introduced for each component, whose value is dependent on the shape and type of the component. The minimum value of the geometry factor is 1, for straight tubes. Moreover, the hydrodynamic effect of a component on downstream components is taken into account by calculating a decreasing factor along the downstream line. The pH, hydrogen and temperature effects have been validated with the CIROCO loop. Finally, the effect of chromium as a paramount parameter to reduce the FAC rate has also been included. All these parameters allowed the authors to propose a simplified model which is:

$$V = 2kf(Cr)c_e \quad (32)$$

where $f(Cr)$ is an empirical function including porosity, hydrogen pressure and chromium content effects according to the temperature.

This simplified model is used for temperatures higher than 50 °C and for Reynolds numbers between 5×10^4 and 1×10^8 . For lower temperatures, some cases of FAC degradation have been described (low temperature FAC) and the model must be redefined to take into account the magnetite formation rate and the mass transfer.

The successes of this approach include:

1. the constitution of a database including an inventory of lines and a determination of initial margins;
2. the evaluation of possible wall thinning kinetics using the deterministic computer program BRT-CICERO Version 1 available on the PC since April 1993;
3. the establishment beginning from 1989 of a programme calling for inspections of a set of control parameters every three years.

The probabilistic approach [19] In order to improve the reliability of the forecasts and optimize the inspection programmes and maintenance operations, it has been considered necessary to apply a probabilistic approach to corrosion-erosion. This is a medium-term approach that takes advantage both of the rather advanced maturity of the physico-chemical model, feedback from the operator's experience, and the fact that the precautions taken in the last fifteen years, in both operation and maintenance, have eliminated all risk of a serious accident [19]. It is therefore a matter of operating reliability. Currently, the EdF approach relies on the software BRT-CICERO available on PC and now in use in every french unit since 1994 [19].

The most important factors on the underthickness probability were identified: initial thickness and chromium content when no chromium measurement on the component is available. The input random variables are given in Table 1. Moreover, the deterministic version allowed the user to take into account thickness measurements for underthickness predictions. Consequently, the probabilistic module had to provide the same capability. That is why a bayesian updating approach was performed. The principle of this approach is to update the underthickness probability and the probabilities $P(Th_{\text{residual}} < \text{threshold})$ giving the

residual thickness distribution by integrating the knowledge of measurements in a probabilistic manner.

Table 1. Input variables in the probabilistic approach of BRT-CICERO code.

Variable		Distribution type
DI	Internal diameter	Normal
x	Power level	Histogram
Cr	Chromium content	Histogram
Th_{ini}	Initial thickness	Beta
Err_{mes}	Measurement uncertainty	Trunc normal
Cb_i	Concentration of the base n ^o i, i = 1 to 4	Lognormal
A	Geometric factor	Beta

This is done by the evaluation of the conditional probability as follows:

$$P(Th_{residual} < threshold / Th_{measured} \in [Th_{mes_inf}; Th_{mes_sup}])$$

where $Th_{residual}$ stands for residual thickness, threshold is a bound of the histogram class of the residual thickness distribution, $Th_{measured}$ is the distribution of measured thickness, Th_{mes_inf} is the lower bound of the measured values and Th_{mes_sup} is the upper bound. The interval size plays an important part: if simulations are used it must be large enough to avoid a huge number of sampled values. This is the case because the on site inspection procedure leads to gridding the component. The location grid consists of lines both perpendicular and parallel to the flow direction. Thickness readings (from Ultrasonic Testing (UT) measurements) are then taken and recorded at the grid intersection points. The grid spacing is normally a function of the component diameter. The major point of the bayesian updating approach is that all the information contained in the measurements is employed, whereas in the deterministic version (version1) the only change was to use the measured values as new initial residual thickness values but without updating the wall thinning kinetics, which led to wrong predictions.

Basic features of BRT-CICERO Version 2 [19] The improvements in version 2 were mainly related to the following:

1. Chromium – the model improvement carried out to take into account the chromium effect is included after several validation tests on the CICERO loop
2. Geometric factors – (1) the table of geometric factors was upgraded in two areas: an analysis of the plant feedback experience. In this case, the selected data consider only components with a known chromium composition and with two or more UT thickness measurements; (2) calculations using a finite element approach;
3. Probabilistic module: as mentioned before, it has been included to reduce uncertainties and conservatisms in the wall thinning predictions. It was supposed to take advantage of a better knowledge of the chromium content distribution for the components without chromium measurement, and also of the real initial thickness distribution;

4. A specific module was also developed to calculate the thermohydraulic parameters involved in the wall thinning kinetics as a function of the power level of the unit, a new input distribution of the probabilistic module.

After BRT-CICERO software enabled the operator to detect a severe damage on an expander downstream of a regulated valve of the unit 2 of Fessenheim in year 2000, the corporate level of EdF decided to make mandatory the use of BRT-CICERO™ for all the 58 NPPs.

The BRT-CICERO™ input-databases [20,21] An input-database is specific to a plant and is built-up for a complete analysis of the degradation by FAC of the secondary circuit main pipes. This input-database contains the pipe isometrics, the material and mechanical pipe characteristics, the hydraulic conditions for each line, the operating times and chemical data for each cycle, the design codes and material standards. In addition, BRT-CICERO™ enables to introduce thickness and chromium content measurement results, obtained during outage inspections. The thickness measurements are performed on pipe elements according to a pre-defined mesh and the results are edited into a specific file format. The in-service measured thickness is used by BRT-CICERO™ as a new reference thickness whereas the chromium content is used in the FAC rate calculation. All of the pipe thickness measurements realized on the French nuclear power plants secondary circuits since the 1986 Surry accident are now available in the input-databases.

Degree of confidence in BRT-CICERO™ After exclusion of the wrong input data that are responsible for artificial non-conservative predictions, T. Knook et al. [21] obtained the curve on Figure 6. Some points appear to be predicted with a high degree of conservatism: this is generally due to a lack of information on the chromium content or to an initial thickness much higher than specified, which is often the case for thick components (headers, tees, large bore reducers). Some cases can also be due to a too conservative geometry factor.

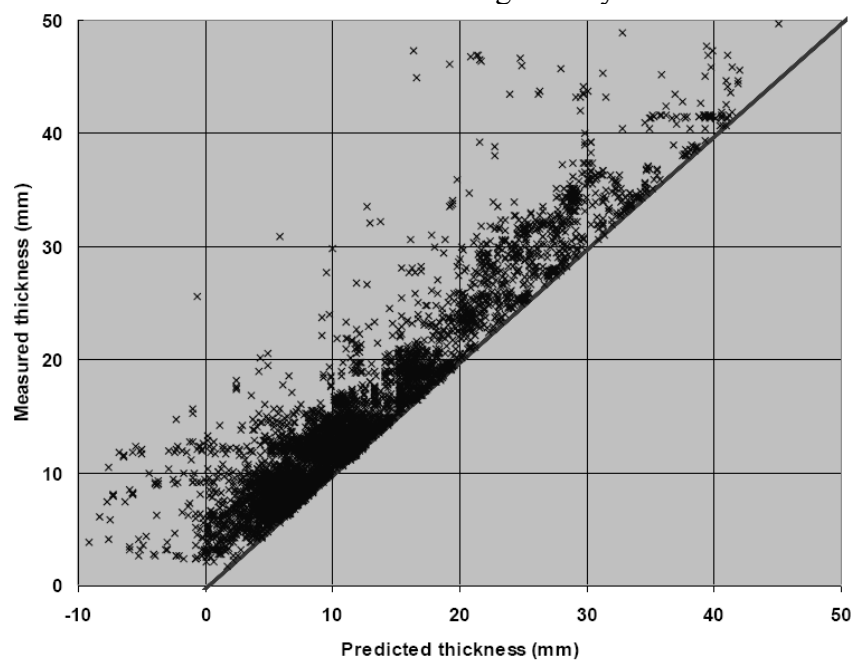


Figure 6 Comparison between measured and calculated components thicknesses according to the BRT-CICERO database.

5.3 Coupling analysis of corrosion and fluid dynamics (CAC-FD)

According to the perspective of this approach proposed by Japanese and Canadian researchers [21], flow accelerated corrosion (FAC) is divided into two processes: the corrosion (chemical) process and the flow dynamics (physical) process. The former is the essential cause of FAC, while the latter accelerates its occurrence.

The authors [21] state that a systematic approach for evaluating FAC is desired before discussing application of countermeasures for FAC. Also, future FAC occurrences should be evaluated to identify locations where a higher possibility of FAC occurrence exists, and then, to predict FAC rates at these locations of interest. The effects of the countermeasures for FAC should also be evaluated along with their adverse effects on materials. The key factor to determine FAC is the oxide film on pipe surfaces, which develops as a result of corrosion and, at the same time, controls the corrosion rate in its role as a protective barrier. According to the CAC-FD approach, the major parameters that influence the extent of FAC and determine its rate can be divided into: material parameters, flow dynamics parameters and environmental parameters, as shown in Figure 7.

As a result of an extensive joint Japanese-Canadian experimental effort [22,27,28], focus was placed on the influence of environmental parameters on FAC in order to determine its main mechanism and to discuss suitable countermeasures based on water chemistry control. Wall thinning evaluation during FAC is based on a time invariant surface electrochemical charge balance together with a transient model for oxide growth and dissolution. According to this concept, the elementary models that have to be combined to evaluate FAC rates are presented schematically in Figure 8.

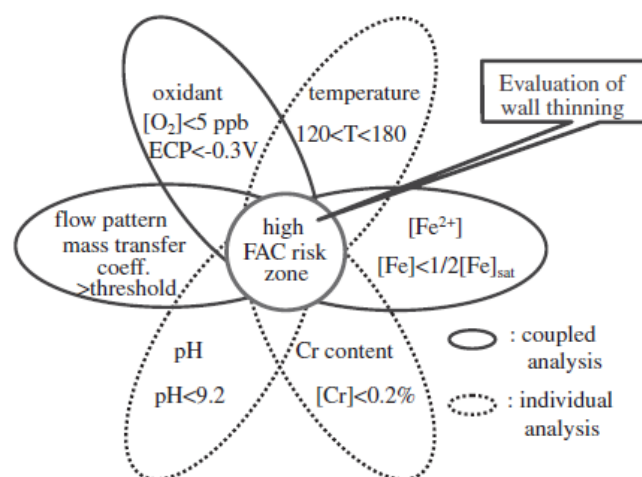


Figure 7 A sketch of the major parameters influencing flow-accelerated corrosion according to the approach proposed by Uchida and co-workers [21-51].

Following the ideas of the CAC-FD approach, metallic ions, mainly ferrous ions (Fe^{2+}), are released into the water at the boundary (or equivalently, diffusion) layer. Due to supersaturation resulting from the low solubility of iron in the medium, certain part of Fe^{2+} are back-deposited on the metal surface to form a magnetite oxide layer. In turn, the oxide layer plays an important role in preventing more Fe^{2+} release (i.e. it slows down the corrosion reaction). The thickness of the boundary layer is strongly affected by flow dynamics. Oxygen

concentration ($[O_2]$) in the diffusion layer also plays an important role in these processes by oxidizing magnetite to maghemite or hematite, resulting in a considerably higher corrosion resistance. Chemistry in the surface boundary layers and its coupling with flow dynamics was analyzed to evaluate FAC rates in a six-steps procedure (Figure 9). The main inputs, outputs and software used in the calculations are summarised in Table 2.

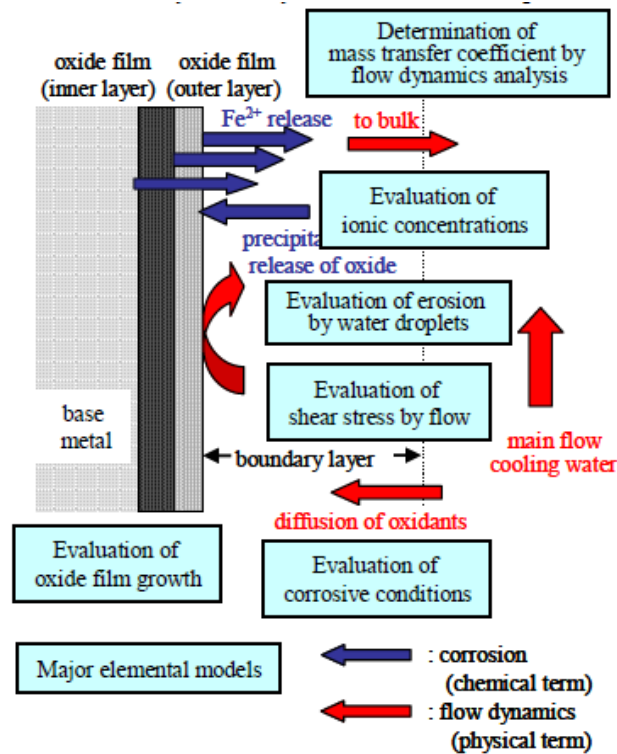


Figure 8 Combination of the elementary processes resulting in FAC according to the CAC-FD approach [22-26].

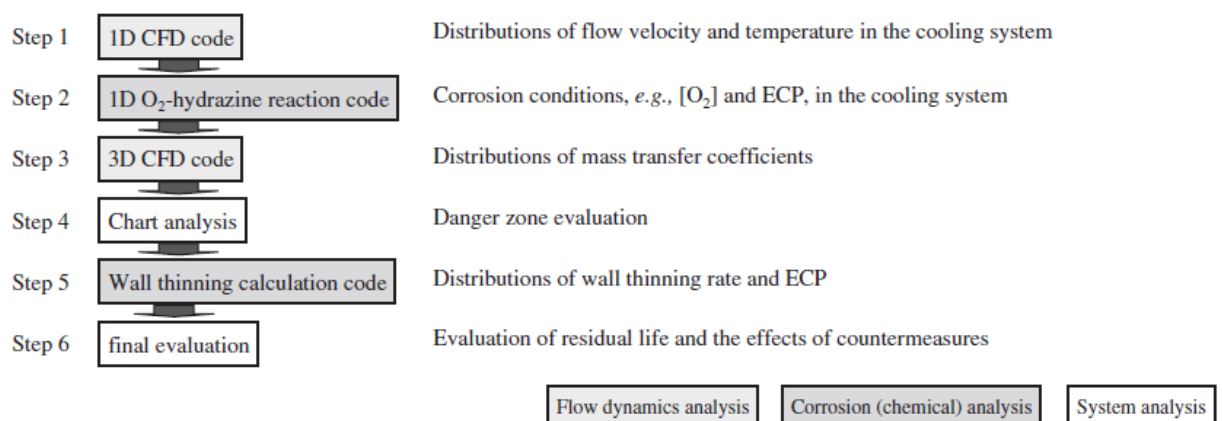
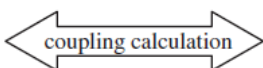


Figure 9 Calculation steps to evaluate FAC rates [25].

First, flow distribution and temperature in each elemental volume along the flow path were obtained with 1-3D computational flow dynamics (CFD) codes in order to assess the thickness of the boundary diffusion layer and mass transfer coefficients between this layer and bulk water. In order to minimise computer time, flow distributions were calculated in the whole system with an 1D CFD code (RELAP5), whereas those in local

regions with complex geometry were evaluated using 2-3D k (turbulent kinetic energy)- ε (energy dissipation rate) codes (PLASHY, α -FLOW) or a 3D LES code. It was confirmed that the k - ε method calculation with the wall functions gave the same results as the large eddy simulation (LES) calculation with lower mesh number and lower CPU time.

Table 2 The system of codes to evaluate the wall thinning rate caused by FAC according to the CAC-FD approach [25].

Calculation targets	Flow pattern	[O ₂], [Fe ²⁺]	Wall thinning rate and ECP (anodic/cathodic current density) (oxide film formation)	
Input	Reactor parameters: geometries, heat flux (Q), temperature (T)	Reactor parameters: T, flow velocity (v), surface/volume rate, mixing rate	[O ₂], T, pH, k_m , oxide film thickness, oxide properties	i_{corr} , ECP
Computer programs	1D CFD (RELAP5) ^{a)-c)} 2-3D k - ε CFD ^{c)} (PLASHY, α -FLOW) 3D LES ^{c)}	N ₂ H ₄ -O ₂ reaction code ^{b)} (RADIOLYSIS-N2H4)	Static model ^{d)} (Electrochemistry)	Dynamic model ^{d)} (Oxide layer growth)
				
Output	T, v distributions along the flow path along the flow path	[O ₂] and [Fe ²⁺] distributions	i_{corr} , ECP wall thinning rate	oxide film thickness oxide properties (Fe ₂ O ₃ /Fe ₃ O ₄ ratio)

^{a)}Step 1 ^{b)}Step 2 ^{c)}Step 3 ^{d)}Step 5

Calculated, precise flow velocity distributions were obtained, which were applied to evaluate friction velocity distribution at the pipe surface, distributions of turbulent energy, k , and then mass transfer coefficient, K_d [28]:

$$k = \frac{u_f^2}{c_\mu^{1/2}}, K_d = u_f \frac{Sh}{ScRe}, u_f = \sqrt{\frac{\tau}{\rho_f}}, Sh = a_1 Re^{a_2} Sc^{a_3}, Re = \frac{\rho_f u_f d}{\mu}, Sc = \frac{D}{\mu} \quad (33)$$

where τ is the shear stress at the solid surface, μ is the dynamic viscosity, ρ_f the density of the fluid, u_f is its velocity and c_μ is a constant.

Next, corrosive conditions, namely, [O₂] and [Fe²⁺] and corrosion potential (ECP) along the obtained flow paths were calculated with an oxygen-hydrazine reaction code, using two types of expressions for the rate of the reaction between oxygen and hydrazine as follows [29]

$$\begin{aligned} \frac{d[O_2]}{dt} &= \frac{d[N_2H_4]}{dt} = 6.84 \times 10^4 e^{-\frac{43000}{RT}} [O_2]^{1/2} [N_2H_4] \quad (\text{bulk reaction}) \\ \frac{d[O_2]}{dt} &= \frac{d[N_2H_4]}{dt} = 9.0 e^{-\frac{28200}{RT}} [O_2]^{1/2} [N_2H_4]^{1/2} \quad (\text{surface reaction}) \end{aligned} \quad (34)$$

A schematic of the cathodic and anodic processes considered, as well as the corresponding Evans diagram, is shown in Figure 10 (above), whereas the so-called “modified double-layer oxide model” is presented in Figure 10 (below). According to the Evans diagram, the cathodic current is determined by reduction reaction of oxidant at the surface, where the oxidant concentration was calculated by its diffusion through surface boundary and oxide layers. The anodic current was determined by the sum of currents due to ferrous ion release from the metal

surface and hydrazine oxidation reaction. Both currents were also determined by the diffusion of products and reactants through surface boundary and oxide layers. As a balance of the anodic and cathodic current densities, electrochemical corrosion potential, ECP, was calculated. The minimum potential was set by the hydrogen evolution potential, which was determined by pH and temperature of the water.

According to the CAC-FD approach, the electrochemistry model determines the static balance of charge at the oxide surface with a given oxide film thickness. On the other hand, the oxide layer growth model expresses the dynamics of the oxide film growth and dissolution, and film thickness is calculated as a result of accumulated mass balance of metal released from the substrate. Ferrous ion release rate from base metal is estimated using the electrochemistry model. Part of the ferrous ions are transferred to the bulk water and others are absorbed on the surface of the magnetite and hematite particles depositing on the metal surface, while the major portion over the supersaturation concentration in the boundary layer precipitate as oxide particles, which deposit on the surface to become an oxide layer (magnetite particles). Magnetite particles are oxidized as hematite on the metal surface. The double layer oxide model is based on the following set of largely empirical equations:

$$\frac{dL_s}{dt} = -\frac{k}{\left[R_m (L_{\min} + L_m) + R_h L_h \right]}, \text{ thinning of the steel}$$

$$\frac{dc_{Fe^{2+}}}{dt} = \frac{k}{\delta_{bl} \left[R_m (L_{\min} + L_m) + R_h L_h \right]} - k_{rel,m} c_{Fe^{2+}} L_m^{2/3} C_m^{1/3} f_m \delta_{bl} - k_{rel,h} c_{Fe^{2+}} L_h^{2/3} C_h^{1/3} f_h \delta_{bl} - \frac{k_g c_{Fe^{2+}}}{c_{eq}} \frac{f_b}{W_m} - K_d (c_{Fe^{2+}} - c_{Fe^{2+},bulk}) + \frac{k_{rel,m} L_m}{\delta_{bl}} + \frac{k_{rel,h} L_h}{\delta_{bl}}$$

(ferrous ion concentration in the boundary layer)

(35)

$$\frac{dc_p}{dt} = \frac{k_g c_{Fe^{2+}}}{c_{eq}} \frac{f_b}{W_m} - k_{diss} c_p - K_d (c_p - c_{p,b})$$

(oxide particle concentration in the boundary layer)

$$\frac{dC_m}{dt} = \frac{k_g c_{Fe^{2+}}}{c_{eq}} \frac{f_b}{W_m} - (\chi + k_{m,m}) C_m$$

(number of magnetite particles in the oxide)

$$\frac{dL_m}{dt} = k_{magn} L_m^{2/3} C_m^{1/3} f_m \delta_{bl}^2 + \frac{k_g c_{Fe^{2+}} f_b \delta_{bl}}{c_{eq}} - (k_{rel,m} + \chi + K_{d,m}) C_m + \chi M_{magn} \left[R_m (L_{\min} + L_m) + R_h L_h \right]$$

(thickness of magnetite layer)

$$\frac{dC_h}{dt} = \chi C_m - K_{d,h} C_h$$

(number of hematite particles in the oxide)

$$\frac{dL_h}{dt} = \chi L_m + k_h L_h^{2/3} C_h^{1/3} f_h \delta_{bl}^2 - (k_{rel,h} + K_{d,h}) L_h$$

(thickness of hematite layer)

(36)

where L_s is the dissolving thickness of the steel substrate, k is the dissolution rate constant, R_m , R_h are “resistance factors” for magnetite and haematite, L_{\min} the

minimum thickness, L_m , L_h are the thicknesses of the magnetite and haematite sublayers, δ_{bl} the thickness of the boundary layer, C_m , C_h are the number densities of particles per unit volume of magnetite and haematite, k_{magn} is the rate constant of magnetite formation, $k_{rel,m}$, $k_{rel,h}$ the release rate constants for magnetite and hematite, k_g – rate constant of generation of magnetite particles in the boundary layer, $K_{d,m}$, $K_{d,h}$ - the mass transfer rates of particles of the respective oxides through the boundary layer, K_d – mass transfer coefficient of ferrous ions in that layer, f_b is a function of the ferrous ion concentration, and f_m , f_h are geometrical factors for magnetite and hematite particles, respectively. The conversion factor from magnetite to hematite χ is expressed as a function of ECP (or equivalently, dissolved oxygen concentration) using an empirical equation linear in $[O_2]$.

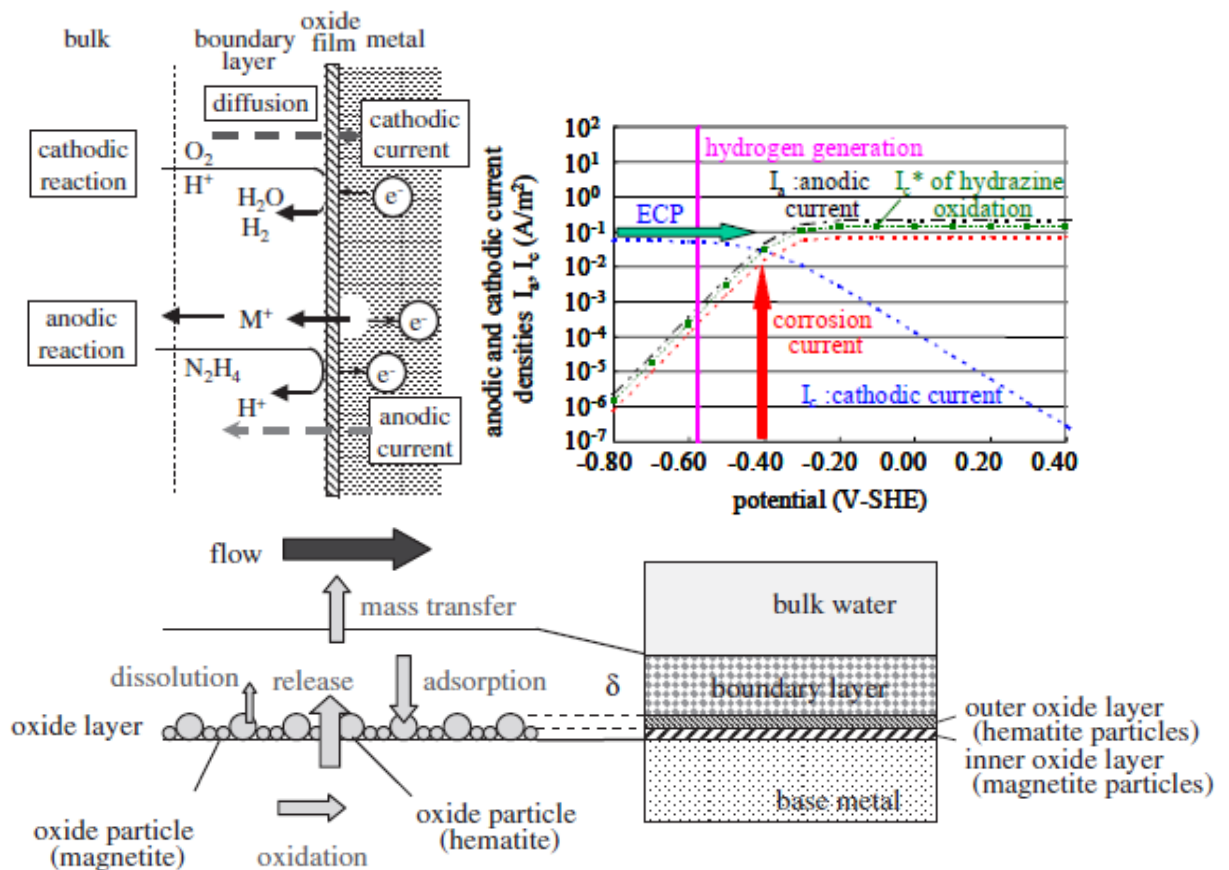


Figure 10 (above) Surface electrochemistry according to the CAC-FD approach; (below) “modified double-layer oxide model” [25].

The interaction between the static electrochemistry model and the dynamic film growth/dissolution model to evaluate the FAC rate is presented in Table 3. Anodic and cathodic current densities and ECP are calculated with the static electrochemistry model and ferrous ion release rate determined by the anodic current density is applied as input for the dynamic oxide layer growth model. The thickness of oxide film (oxide layer) and its characteristics are applied for the electrochemistry model to determine the “resistance” to the cathodic current from the bulk to the surface and anodic current from the surface to bulk (perhaps the authors have in mind the respective polarisabilities of the anodic and cathodic process). The model has been found to reproduce to a first approximation the experimental dependences of the corrosion rate on the mass transfer coefficient

and pH (Figure 11), although further experimental efforts from the Japanese-Canadian cooperation seem to demonstrate that at higher pH values (above 9.2) the reaction is not completely mass-transfer controlled anymore because of the reduced solubility of magnetite [28].

Table 3 Coupling between surface electrochemistry and oxide layer growth/dissolution.

	Electrochemistry model (static)	Oxide layer growth model (dynamic)
Major points	anodic/cathodic current density	oxide film formation
Input	oxidant concentration, temperature, pH, mass transfer coefficient, oxide film thickness, oxide properties	corrosion current density ECP
Output	corrosion current density, ECP, wall thinning rate	oxide properties ($\text{Fe}_2\text{O}_3/\text{Fe}_3\text{O}_4$ ratio)

The target accuracy for the evaluation model for pipe wall thinning due to FAC has been confirmed by comparison of the code calculations with plant data (Figure 12). Despite the relative success of the code, there are several conceptual drawbacks in the coupled surface electrochemical – oxide growth/dissolution model:

- it is assumed that at low oxygen concentrations, the cathodic current density is low and the anodic current density is high because of the assumption that molecular oxygen is needed for film growth, which is at odds with contemporary understanding of film growth mechanisms in high-temperature water (in fact, magnetite films grow also at low potentials in deoxygenated conditions since there is plenty of water to oxidise the metal).
- The only mechanism for film growth and restructuring that is assumed operative is the dissolution-precipitation mechanism, i.e. in spite of the bilayer model considered, the existence of a barrier layer growing on the steel surface by a solid-state mechanism is not taken into account. It has been demonstrated in the recent literature that the corrosion properties of carbon and stainless steel in high-temperature water are most probably controlled by the properties of the thin barrier layer that grows via a sequence of solid-state reactions. These findings need to be incorporated in the model in order to take into account the film growth/restructuring more accurately and thus make the predictions of the model more realistic.
- The so-called “modified double-layer model” uses several empirical relationships as governing equations, e.g. the conversion factor of magnetite to hematite is written as a linear function of oxygen concentration, the rate of increase of hematite and magnetite thicknesses with time is taken as proportional to the thickness at a power of 2/3, etc. The effect of the oxide film on the anodic current density is also taken into account in an empirical way via oxide resistivities that influence the polarisability of the anodic reaction.

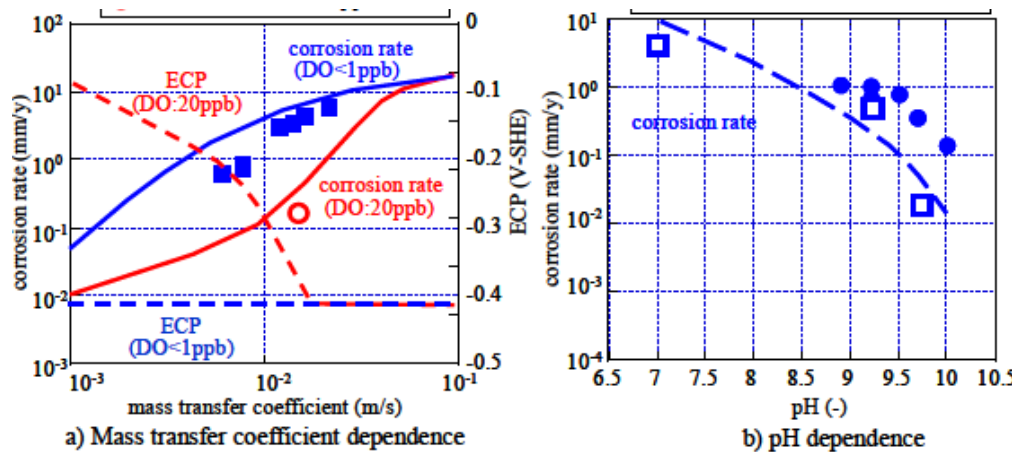


Figure 11 Corrosion rate as depending on mass transfer coefficient and pH. Points – experimental values, lines – calculational results.

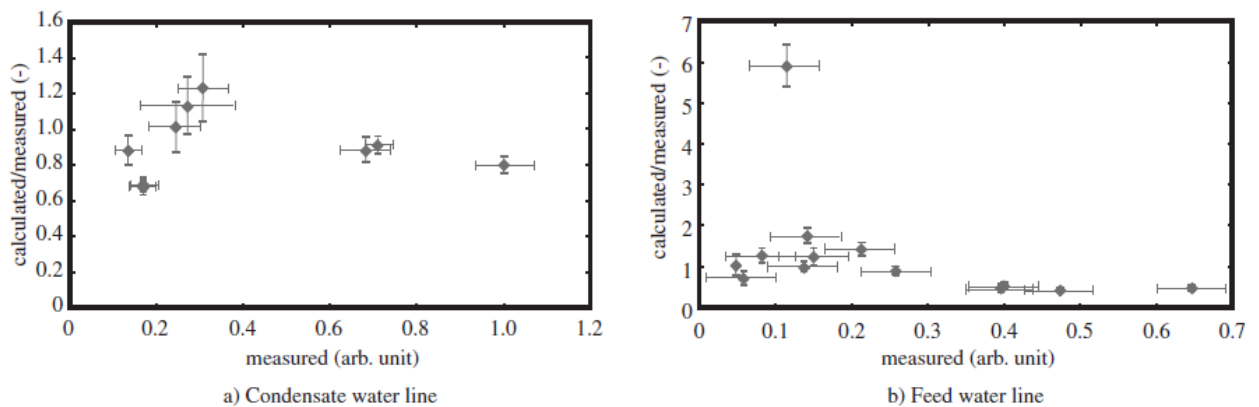


Figure 12 Relationships between measured values of FAC rates and those calculated by the code [25].

5.4 Local flow approaches to the two-phase flow-accelerated corrosion

Two phase flow-assisted corrosion, as yet another aspect of erosion/corrosion, is a process of piping degradation that is caused by the flowing fluid (water-steam mixture) disrupting or thinning the protective film of corrosion products [31-35]. In analogy to single-phase FAC, two-phase FAC is a combination of two major processes: electrochemical corrosion, i.e. dissolution of the oxide layer on carbon steel pipe walls, and mechanical erosion accelerated by high-velocity liquid droplets impinging on the wall. Experimental observations or plant measurements strongly reveal that this type of FAC also depends on the piping layout, local distributions of flow properties, flow chemistry, etc. Consequently, the process is characterised by multidimensional behaviour, especially in its location distributed around the pipe walls. Local flow structures are found to interfere with the formation of protective films and affect the mass transfer rates of corrosion reactants through the boundary layer. In addition, multidimensional characteristics of the wear pattern are shown in experimental results and plant data, rendering the need for a multidimensional model to examine the FAC local phenomenon. To

describe this, the authors [31-35] propose a model that has two essential parts: the droplet impingement erosion model and a mass-transport controlled corrosion model. Both models are used to treat the two-phase system, but only the mass-transport controlled corrosion model is used for the single-phase FAC.

The two-phase system simulated is a high-quality steam system with a flow quality of 85 to 92%; the size of the liquid droplet is sufficiently small, and the droplet can be carried by high-velocity steam. A liquid droplet with enough high kinetic energy will impinge on the oxide layer of metal and erode its wall surface, leading to the occurrence of FAC.

According to the proposed erosion submodel, the oxide layer formed on the carbon steel surface is removed by the action of numerous individual impacts of the liquid droplet, resulting in a phenomenological equation for the wear rate (m) of the type

$$m = CNF(\theta) \frac{\rho_f u_f^2}{H_v} \quad (37)$$

where C is a constant for a given two-phase system, H_v is the hardness of the pipe wall, N is a characteristic frequency of impingement, $F(\theta)$ is a function of the angle of impact, ρ_f the density of the liquid (or equivalently, the concentration of liquid droplets) and u_f is the vector of the normal velocity of the two-phase fluid. Based on comparison of plant measured information and focusing on the distribution of sites of FAC wear damage, the authors [31-35] propose a simplified parameter $\alpha_f \mu_f |u_f|$ to be an appropriate indicator of the magnitude of erodent kinetic energy. In this form, α_f is the volume fraction of the liquid droplet, and $|u_f|$ the magnitude of the fluid velocity vector.

Assuming that the total reaction is completed on the pipe walls, and its rate is dominated by the ion production rate r_p and ion transfer rate, the electrochemical corrosion submodel expresses r_p in a simplified form as

$$r_p = 2k_p (c_{eq} - c_w) \quad (38)$$

where k_p is the reaction rate constant, c_{eq} - the equilibrium ferrous ion concentration and c_w - the actual concentration of that ion at the oxide/fluid interface. The ferrous ion is generally distributed with the flowing fluid so that the profile of ions coincides with that of the flowing fluid. Lower local near-wall fluid velocity will cause a steeper radial profile of flowing fluid, increase the gradient of soluble ferrous ion concentration, and consequently enhance the local corrosion production rate and promote the metal loss of the pipe wall. Near-wall fluid velocity is then again an indicator to express the possible distribution of FAC locations.

In turn, the ferrous ion transfer rate is represented as

$$r_m = K_d (c_w - c_b) \quad (39)$$

where K_d is the mass transfer coefficient and c_b the concentration of ferrous ions in the bulk of the fluid. The mass-transfer coefficient is a function of the

dimensionless characteristics of the fluid mass transport properties (Sherwood, and accordingly Reynolds and Schmidt numbers) according to

$$K_d = \frac{ShXD}{d}, Sh = a_1 Re^{a_2} Sc^{a_3}, Re = \frac{\rho_f u_f d}{\mu}, Sc = \frac{D}{\mu} \quad (40)$$

where D is the diffusion coefficient of the ferrous ion and a_i ($i=1..3$) are empirical constants. When the steady-state is reached in a fully developed pipe flow, the rate of production and transfer of ferrous ion should become equal, and the total metal loss rate will then be expressed as

$$r = \frac{c_{eq} - c_{bulk}}{\frac{1}{2k_p} + \frac{1}{K_d}} \quad (41)$$

For the sake of the validation of the model, the fluid system at the secondary side of a NPP has been divided into six major systems - the main steam, feedwater, condensate, turbine, turbine exhaust and drain, and steam generator blowdown systems. Because the geometry of the simulated pipes is not of a simple rectangular or cylindrical system, a body-fitted coordinate method has been adopted to deal with the multidimensional geometry. The governing equations describing the two-phase flow have been discretized by a finite-difference approach, whereas the hybrid scheme has been employed to treat the convection terms coupled with the diffusion terms. The coupled equations for the velocity and pressure have been solved by the interphase slip algorithm which is a two-phase extension of the SIMPLE scheme [33] for a single-phase flow. According to the authors [33-35], several computational flow codes can be applied to solve this problem; these include TEACH, PHOENICS, and FLOW3D [37-39].

The model calculations presented in the paper [33-35] demonstrated that the behaviour of liquid droplets is strongly influenced by centrifugal and gravitational forces, which can be accurately estimated, including the droplet's being pushed to the outer side of the elbow because of centrifugal force and falling, thereby accumulating at the bottom of the pipe under the influence of gravitational force as the two-phase mixture passes along a horizontal pipe. Compared with the plant measured data, the FAC locations predicted by the proposed indicators (essentially derived from the physical phenomena of droplet impingement erosion and chemical corrosion) have shown satisfactory agreement. In addition to the distributions of location of serious FAC, the wear characteristics influenced by the upstream fitting, flow direction, and external forces have been claimed to be captured by the model [33-35]. On the other hand, the influence of flow chemistry, temperature and type of steel material on FAC have not been treated within the frames of the proposed approach.

5.5 Combination between calculation codes and monitoring

It is well known that inspection of all carbon steel piping for PWRs requires excessive time because the associated network of the secondary cooling system is very extensive. Therefore, FAC susceptible regions are usually screened by FAC prediction programs, then ultrasound technique (UT) is employed to inspect those FAC active locations as predicted by the software. However, the prediction of these programs has often been found to contain significant uncertainties, and even

with the screened locations, UT inspection requires time-consuming procedures on point-by-point basis. In some cases, several thousands of components have been selected for thickness inspection by typical FAC management software. However, only about 500 components can be typically inspected during plant refuel outages, thus faster inspection techniques are needed.

Direct current potential drop (DCPD) techniques have been widely used in metallic materials degradation measurement and on-line monitoring, with the proven advantage of relatively high process speed. In the Korean FAC management programme [40-42], it has been shown that DCPD can be employed to rapidly monitor piping wall loss. The FAC screening and inspection approach based on the DCPD technique is presented in Figure 13.

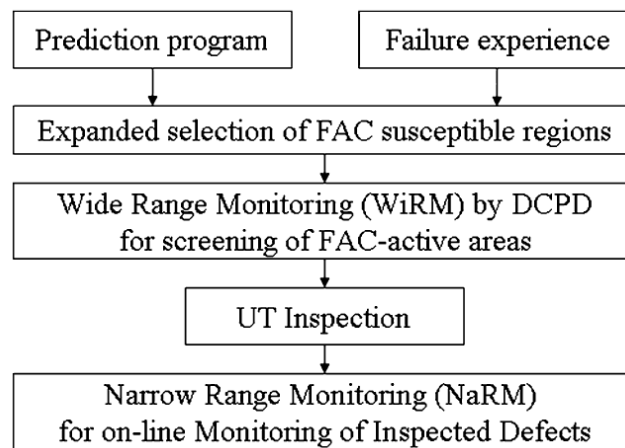


Figure 13 Korean FAC screening and inspection approach [41].

First, piping locations that are likely to be susceptible to FAC are listed by conventional FAC prediction programs with the final selection of high priority locations for UT inspection coverage. Piping segments that are not covered by UT can be further screened by the Wide Range Monitoring (WiRM). If WiRM results suggest the presence of FAC-active areas, then, UT inspections can be extended to increase the reliability of the carbon steel piping network (Figure 13).

During development of the Korean approach based on both an advanced sensor and an evaluation algorithm to monitor FAC, the FAC accelerating parameters were thoroughly examined. ECP and pH were chosen as parameters, which are indirect but globally held parameters to inform us of corrosion susceptibility. Since electrochemical parameters are not a direct measure of the thickness, one more parameter which can be directly affected by thickness reduction was chosen, namely, the amplitude and characteristic mode of piping vibration. To validate the procedures in a test environment, direct thickness measurement using UT has been adopted.

According to the Korean approach, electrochemical parameters are not quantifiable in terms of pipe wall thinning. Therefore, a wearing rate model is introduced to convert monitored variables to thickness information and then compared the result with other sensors [39]. In this case, the Sanchez-Caldera model was used in a modified form according to the equation [43]

$$\frac{dm}{dt} = k_g \frac{\theta(c_{eq} - c_{bulk})}{\frac{1}{k} + (1-f)\left(\frac{1}{K_d} + \frac{\delta}{D}\right)} \quad (42)$$

where the geometrical factor k_g has been introduced to tackle more complex geometry. This factor has been assigned a value of 7.5 for an elbow according to the earlier work of Kastner and Riedle [44]. Solubility of magnetite as a function of temperature has been estimated from the work of Sweeton and Baes [44] and the thermodynamic data for ferrous ions were calculated with HSC Chemistry code [46].

The main contribution of this approach is therefore the introduction of a equipotential switching DCPD measurement of pipe wall thinning using a simple electric resistance model as per the equation

$$\frac{\Delta R}{R_0} = \frac{b}{L} \left(\frac{a/t}{1-a/t} \right) \quad (43)$$

where b is the width of the pipe wall defect, L the probe spacing, a is the depth of the defect and t the thickness of pristine piping. To extend this to cylindrical piping, the angle of defect distribution on the circular wall, Θ , has to be introduced according to the expression

$$\frac{\Delta R}{R_0} = \frac{b}{L} \left(\frac{a\Theta/t}{A - a\Theta/t} \right), \quad A = \frac{1 + t/d}{1 - a/d} \quad (44)$$

where d is the inner diameter of the piping. On the overall, this method gave reliable thickness results that could be successfully compared to the predictions of the Sanchez-Caldera model as shown in Figure 14 together with the maintained electrochemical conditions in the laboratory test loop [42]. As the authors themselves note, however, the ES-DCPD signal in the field can be interfered with slight variations of a detecting location in the case of pipes' vibration, thus a development of a compact fixture of the probes is required for long-term application. Also, the changes in pH deeper in the magnetite stability region and kinetic hindrances of the oxide dissolution also become an important factor that is beyond the predictive abilities of the simple model used in the Korean approach.

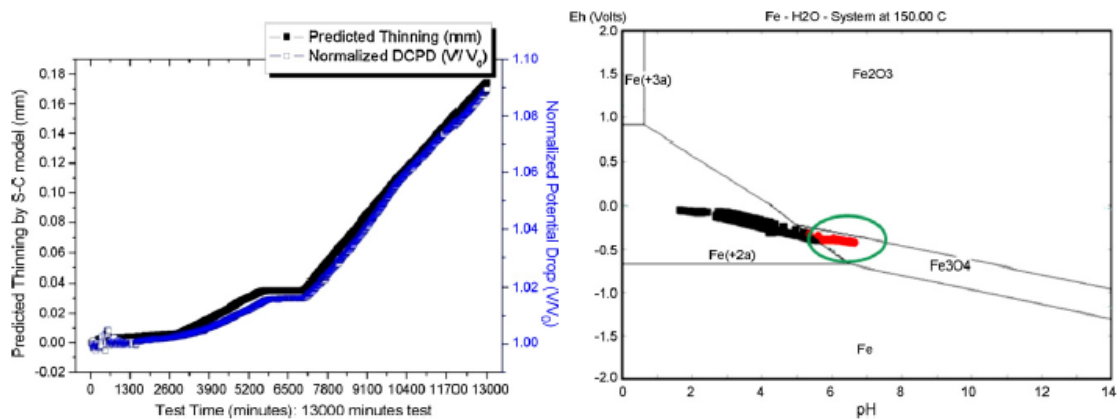


Figure 14 (left) comparison of the measured ES-DCPD results and predicted thinning rate calculated using Sanchez-Caldera model together with the relevant electrochemical conditions in a Eh-pH diagram (right).

5.6 Approaches to FAC modelling in PHWRs

The Pressurized Heavy Water Reactor (PHWR) comprises of a number of horizontal channels containing nuclear fuel bundles. The parallel channels are connected to headers at the inlet and outlet through feeder pipes. The carbon steel outlet feeders carry high temperature water to the headers and from headers, high temperature water goes to steam generator where steam is produced. Due to high velocity, high pressure and temperature, feeders are liable to undergo FAC [47].

Goyal et al. [47] report on an application of KWU-KR model incorporated in the WATHEC software (see above, paragraph 5.1, and also [48]) to two sample geometries and compare the results with those obtained using a shear stress model. The hydrodynamic parameters studied have been the wall shear stress and flow velocities under single phase flow for different geometric configurations. Wall shear stress has been evaluated for steam inlet elbow and outlet feeder. Location of maximum wall shear stress has been claimed to depend upon the inlet and outlet flow condition. According to the authors' [47] interpretation of the model, the rate of FAC can be expressed as follows

$$\begin{aligned}
 r &= 6.35k_g \left\{ Be^{N.u_f} \left[1 - 0.175(pH_{25^\circ C} - 7)^2 \right] 1.8e^{-0.118[O_2]} + 1 \right\} f(t) \\
 B &= -10.5\sqrt{[Cr] + [Mo]} - 9.375 \times 10^{-4} T^2 + 0.79T - 132.5 \\
 N &= -0.0875([Cr] + [Mo]) - 1.275 \times 10^{-5} T^2 + 1.078 \times 10^{-2} T - 2.15 \\
 f(t) &= 0.9999934 - 3.356901 \times 10^{-7} t - 5.624812 \times 10^{-11} t^2 + 3.849972 \times 10^{-16} t^3
 \end{aligned} \tag{45}$$

where k_g is the geometry factor, u_f the fluid velocity, $[O_2]$ - concentration of oxygen in the fluid, $[Cr] + [Mo]$ - contents of Cr and Mo in the steel (%). The geometry factors for different pipe configurations are listed in Table 4.

Table 4 Geometric factors for a range of configurations according to the KWU-KR model (Keller factors).

Behind junctions	0.15
Elbow R/D = 2.5	0.23
Elbow R/D = 1.5	0.30
Elbow R/D = 0.5	0.52
In and over blades	0.30
In branches # 1	0.75
In branches # 2	0.60
On tubes, on blade, on plate	1.0
Leaky joints, labyrinths	0.08
Behind tube inlet	0.16

As an alternative to the KWU-KR model, a hydrodynamic approach has been considered that links the corrosion rate to wall shear stress [47] according to a correlation proposed by Lister et al. [28]. According to this approach, momentum transfer is the physical force within the fluid acting through turbulence at the solid metal surface, which is measured by τ , the wall shear stress. This parameter is a direct measurement of viscous energy loss within the turbulent boundary layer

and is related to the intensity of turbulence in the fluid acting on the wall. The wall shear stress for a given flow velocity (u_f) can be expressed as

$$\tau = 0.04 Re^{-0.25} \rho_f u_f^2 \quad (46)$$

valid for Re from 5000 to 10^5 . Following the literature, the authors state that the majority of the changes in fluid stress characteristics, turbulence, mass transfer and fluid interaction at the wall occur within the boundary layer [49]. At low velocities, the corrosion rate is completely or partially mass transfer controlled. In such a case, the global dissolution at the solid-liquid interface is in a steady-state and the corrosion process is limited by the diffusion of dissolved species in the laminar sublayer from the solid-liquid interface to the bulk fluid, whereas at higher velocities, erosion-corrosion may occur if the wall shear stress is high enough to strip the protective film from the surface [47]. To solve the hydrodynamic equations of their model, the authors [47] use a standard k- ϵ turbulence model with wall functions to improve computing time. In turn, the following correlation has been used for the dependence of the corrosion rate (expressed as depth of corrosion penetration, m) on wall shear stress

$$m = 7.65 \left(1 + 0.111 \tau^{0.75} \right) \left(1 + 1.51 \times 10^{-9} e^{1.87 pH} \right) \quad (47)$$

The following cases have been considered:

<u>Case 1: Steam Generator Inlet Elbow</u>		<u>Case 2: Outlet Feeder Pipe</u>	
Pipe diameter, D	= 428 mm	Pipe diameter, D	= 50 mm
Bend radius, R	= 762 mm	Bend radius, R	= 200 mm
Bend angle	= 90°	Bend angle	= 90°
Inlet Velocity	= 13.7 m/s	Inlet Velocity	= 13.7 m/s

As a result of this comparative study (Figure 15), it has been found that the corrosion penetration in the pipe wall is of the same order of magnitude for both models, the fluid velocity effect being more significant when using the hydrodynamic model. Further monitoring efforts have demonstrated the need to implement an exhaustive and systematic, periodic inspection program, criteria for simulation grid size and adopting a system for recording the inspection data and their residual life analysis [50].

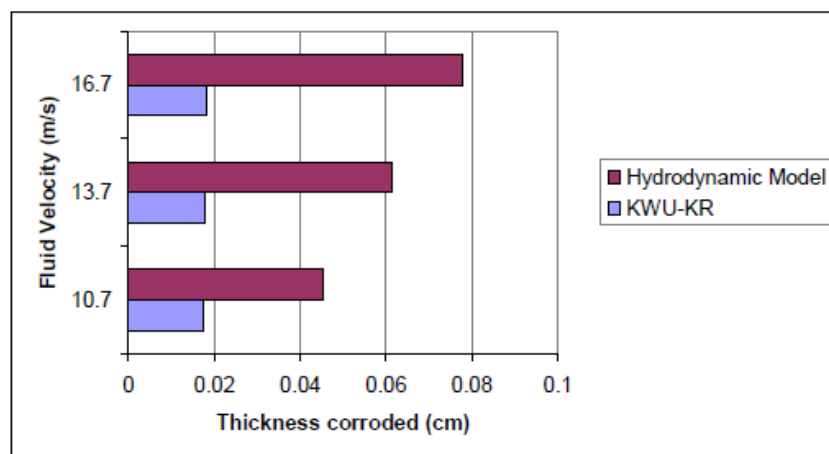


Figure 15 Comparison between the corroded wall thickness calculated using the KWU-KR model and the wall shear stress model [47].

Besides the theoretical developments, researchers that investigated FAC in CANDU reactors [51] have found it necessary to develop probabilistic models and calibrate them using the wall thickness measurements available from CANDU stations. The model has been used to derive a probability distribution of feeder lifetime that was thought to be useful in developing a risk-based criterion for feeder replacements.

The main assumption of the model is that FAC is a slow, incremental process of mass loss by electrochemical and diffusion reactions resulting in the erosion of pipe wall thickness. Such degradation can be conceptually modeled as a stochastic process. If the damage increments are independent and identically distributed, the cumulative damage Y is then assumed to be a gamma distributed random variable

$$f_Y(x) = \left(\frac{x}{\delta}\right)^{n-1} \frac{e^{-x/\delta}}{\delta \Gamma(n)} \quad (48)$$

where δ is the average amount of damage per increment n . The uncertain arrival of shocks (or incremental discrete damages) can be modelled as a Poisson process so that the number n can be taken as a Poisson distributed random variable. The limiting form of it is obtained when the rate of damage occurrence approaches infinity in any finite time interval as the size of the increment tends to zero. Such a process is a gamma-process, within the frames of which the total damage at time t , $X(t)$, is gamma distributed

$$f_{X(t)}(x) = \left(\frac{x}{\delta}\right)^{\eta t-1} \frac{e^{-x/\delta}}{\delta \Gamma(\eta t)} \quad (49)$$

where δ and η are model parameters. The damage increment $\Delta X(t)$ is taken as independent of $X(t)$ and is assumed to be also gamma-distributed

$$f_{\Delta X(t)}(x) = \left(\frac{x}{\delta}\right)^{\eta \Delta t-1} \frac{e^{-x/\delta}}{\delta \Gamma(\eta \Delta t)} \quad (50)$$

The average rate of deterioration per unit time ($\Delta t=1$) is $\eta\delta$ and its variance is $\eta\delta^2$. To account for the dependence of FAC rate on flow velocity, the damage increment (or the scale parameter) δ is modeled as a power function as suggested from empirical studies [52]

$$\delta = \alpha u_f^\beta \quad (51)$$

An additional model parameter is introduced in the incubation time for FAC, adding up to four governing variables including the aforementioned η (shape variable), α and β (scale variables). The end of service life is defined as the time when a critical limit or a threshold value x_F is exceeded. Then the lifetime distribution is obtained as

$$F_T(t) = 1 - \int_0^{x_F} \left(\frac{x}{\delta}\right)^{\eta t-1} \frac{e^{-x/\delta}}{\delta \Gamma(\eta t)} dx \quad (52)$$

The end of life of a feeder is defined by the authors [50] as the time at which the wall thickness is less than 60% of the initial thickness. A feeder that has reached such thinning is defined as a substandard feeder, and the probability distribution of such feeders as a function of the effective full-power years (EFPY) calculated by the model is demonstrated in Figure 16. The authors conclude that the gamma

process with independent damage increments is able to capture the temporal uncertainty associated with FAC.

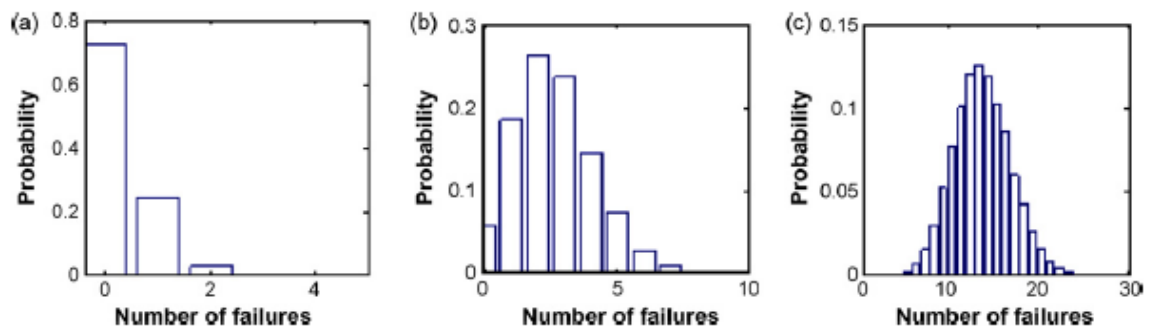


Figure 16 Probability distribution of the number of substandard feeders: (a) 18 EFPY, (b) 19 EFPY, (c) 20 EFPY [51].

5.7 Prediction of FAC rates using the Russian codes RAMEK and ECI

On the basis of long-term investigations a flow-assisted corrosion computational model (RAMEK) has been developed in Russia. RAMEK takes into account physico-chemical processes and regularities, allows estimating and predicting local FAC [53-55]. As mentioned already above, FAC occurs in both single- and two-phase (wet steam) flows. According to the authors [55], there are substantial differences in the mechanism by which the process takes place in the two types of media, as illustrated in Figure 17.

According to the view of the authors, it can be assumed with sufficient accuracy that the parameters determining the nature and the intensity of the corrosion factor (pH, conductivity, concentration of oxygen, iron-containing compounds, alkalization additives, impurities, etc.) slightly change over the section and along the channel in a single-phase water flow. In other words, when modeling processes of metals FAC in single-phase water flow, it is quite possible to use the parameters values of the water chemistry averaged along the flow. Conversely, under conditions of a wet-steam flow, the mechanism of FAC is determined by local values of the physico-chemical parameters and characteristics of corrosion processes (the pH, conductivity, etc.) and hydrodynamic conditions (Re_{film} , Re_{steam} , etc) in the liquid film and in the two-phase boundary layer near the wall. As a consequence of the interphase redistribution of the gases and the impurities, the local values of the pH of the liquid film may considerably differ from the mean value of the pH for the flow (according to the authors' view, they will be lower). Thus the methods for calculating the mass transfer coefficient in the liquid film are not completely analogous to those in a single-phase flow.

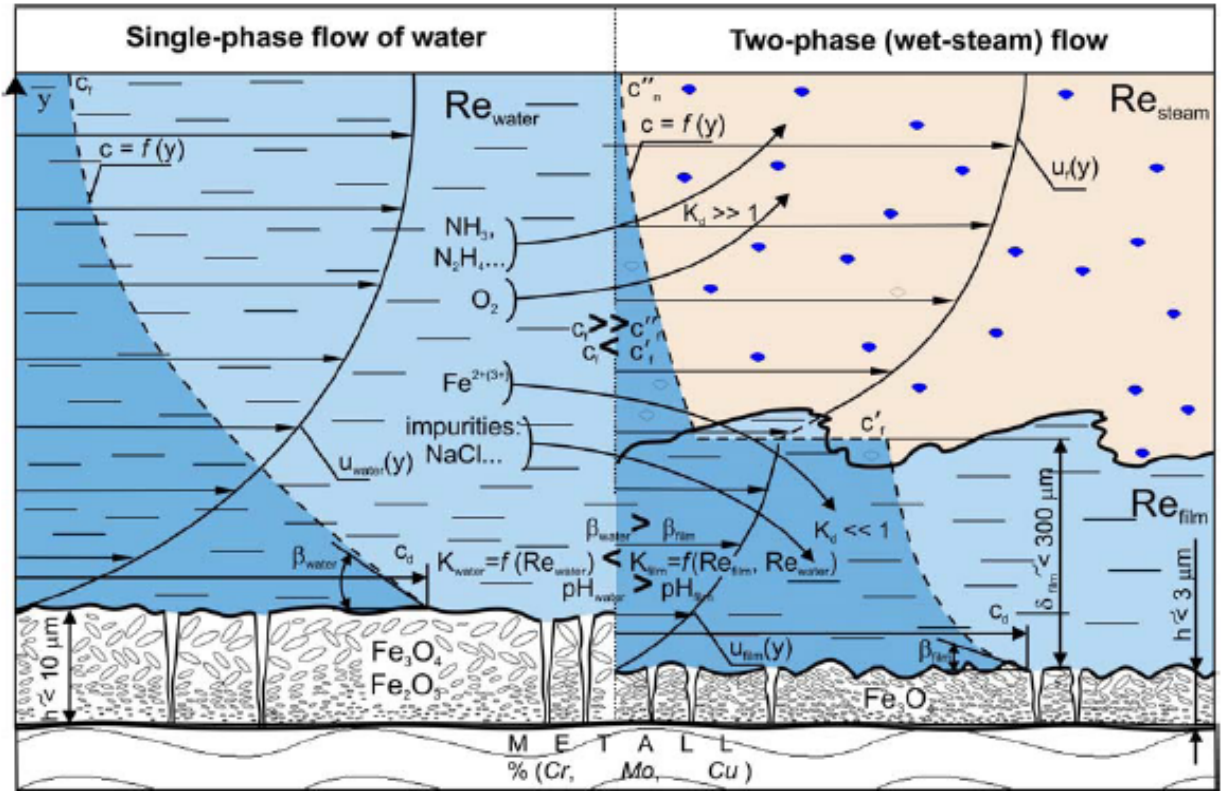


Figure 17 Features of the physico-chemical processes during FAC in single- and two-phase flow [55].

According to the proposed approach, in specific water chemistry conditions, the mechanisms of metal thinning are proposed to differ mostly by the nature of erosive constituent, i.e. hydrodynamic factors. To illustrate that, kinetic curves of main degradation mechanisms, i.e. corrosion in a laminar flow, erosion-corrosion with a convective mass transfer type and erosion with dominating mechanical metal degradation, are summarised in Figure 18.

According to the RAMEK model, the rate of erosion-corrosion (or equivalently, FAC) due both to convective transfer of soluble divalent Fe caused by fluid velocity gradients and vortical transfer due to the energy of turbulent pulsations is defined as

$$r^I = (k_{conv} + k_{vor}) \rho (c_{layer/water} - c_{bulk}) \quad (53)$$

with k_{conv} and k_{vor} the convective and vortical mass transfer coefficients. Besides the loss of metal due to mechanical peeling-off of the oxide layer is presumed to be defined as

$$r^{II} = k_H (\tau_0 - \tau_{extr}) \quad (54)$$

where τ_0 and τ_{extr} are the wall shear stress and its extreme value that results in a mechanical peeling-off, and k_H is a constant. The coefficients k_{conv} , k_H and k_{vor} depend on water chemistry, thermodynamic and other parameters of the flow. The total amount of dissolved ferrous ions due to erosion-corrosion is defined as the sum of equations (53) and (54).

The RAMEK model takes into account most of the major parameters and criteria of FAC: both corrosion and erosion constituents, i.e. metal composition and properties of corrosion products, water chemistry conditions, characteristics of single- and two-phase flows, determining mass-flow peculiarities in near-wall region and mass transfer coefficient values [55,56].

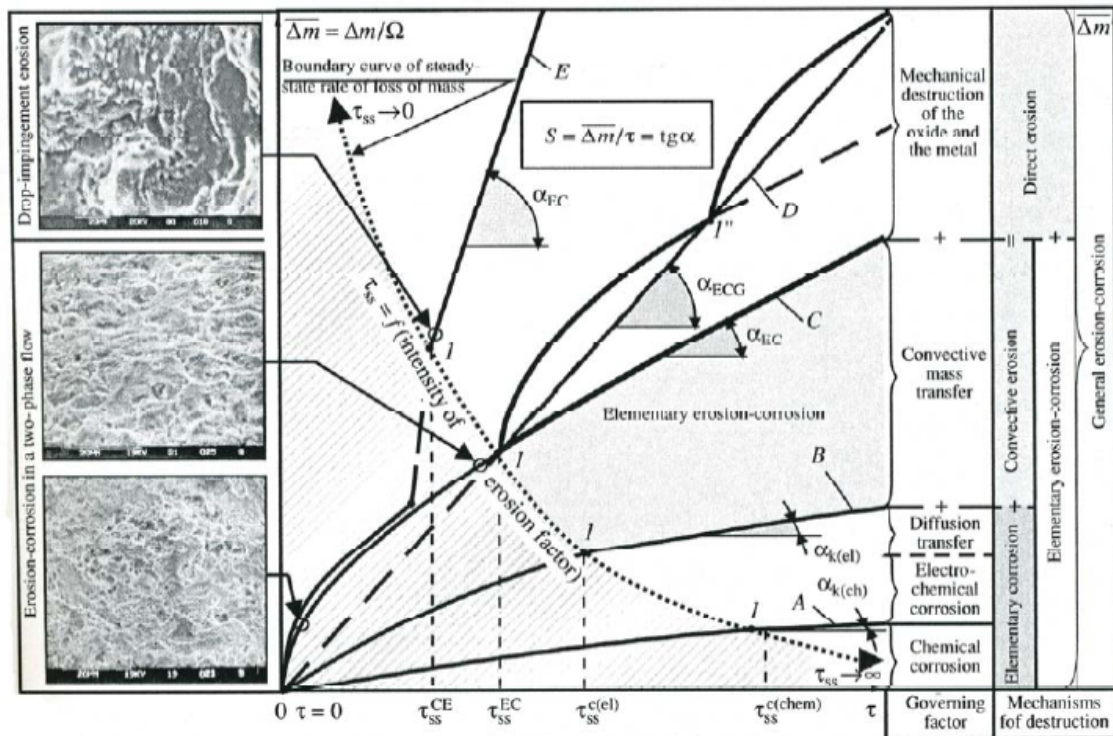


Figure 18 Kinetic curves of degradation mechanisms as depending on the type of the prevailing hydrodynamic effect [56].

The results of computational investigations of the influence of wet-steam flow hydrodynamic parameters on FAC rate at 170 °C have been found to be in line with the tendencies observed in experimental investigations (Figure 19). A growth in the FAC intensity in a wet-steam flow has been noted when increasing the Reynolds numbers of both the steam flow and the liquid film. This effect has a clearly expressed physical characteristic determined by mass transfer of corrosion products. The zones I-III of different FAC thinning rates correspond to the typical liquid film flow conditions: laminar, turbulent and droplet impingement, respectively.

Within the RAMEK code, improvement of accuracy and reliability of the prediction of local wall thinning rates due to erosion-corrosion is thought to be achieved by correct identification of the dominating hydrodynamic factor or contribution of each of these factors to the thinning process. For the purpose, the functional forms of the dependences of the wall thinning rate on the derivatives of the flow rate and the turbulent energy over pipe radius, as well as on wall shear stress, have been obtained on the basis of numerical treatment of experimental data. As an example, the dependence of dimensionless wall thinning rate on du_f/dr is shown in Figure 20. The results of RAMEK calculations have permitted the estimation of the effects of various geometry upstream sections

upon location of the susceptibility zones and relative rate of local erosive-corrosive thinning of pipes, as shown in Figure 21.

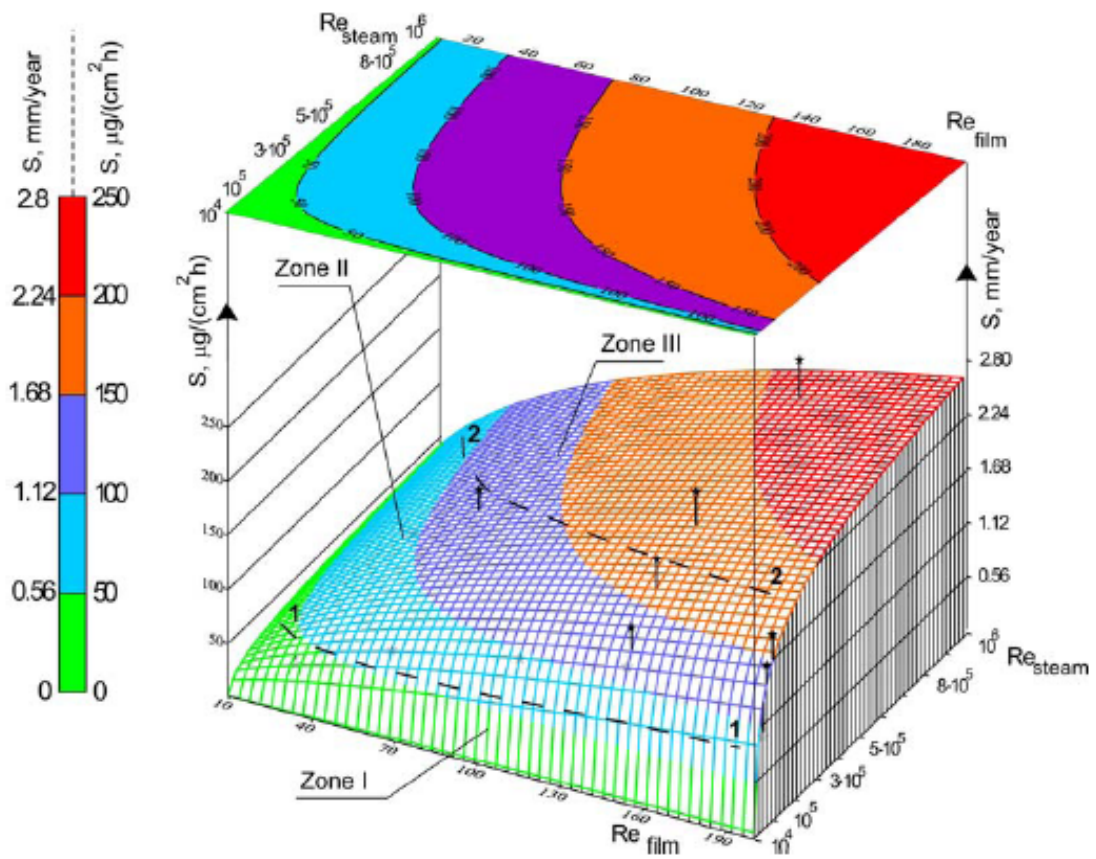


Figure 19 Dependence of the FAC wall thinning rate on the liquid film and steam hydrodynamics according to the RAMEK code.

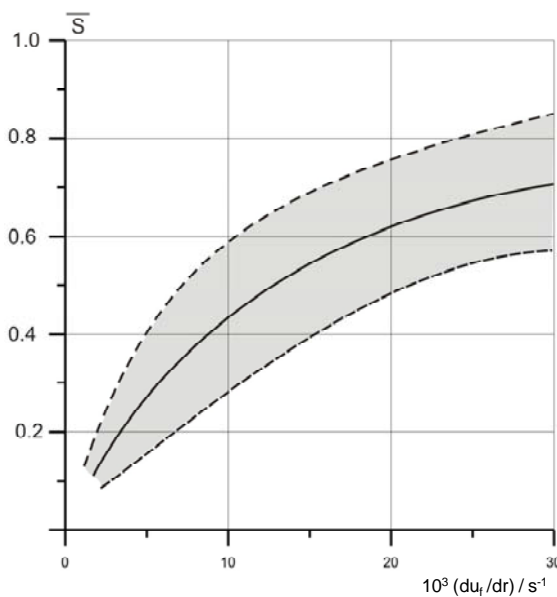


Figure 20 Dependence of the dimensionless local erosion-corrosion factor on du_f / dr .

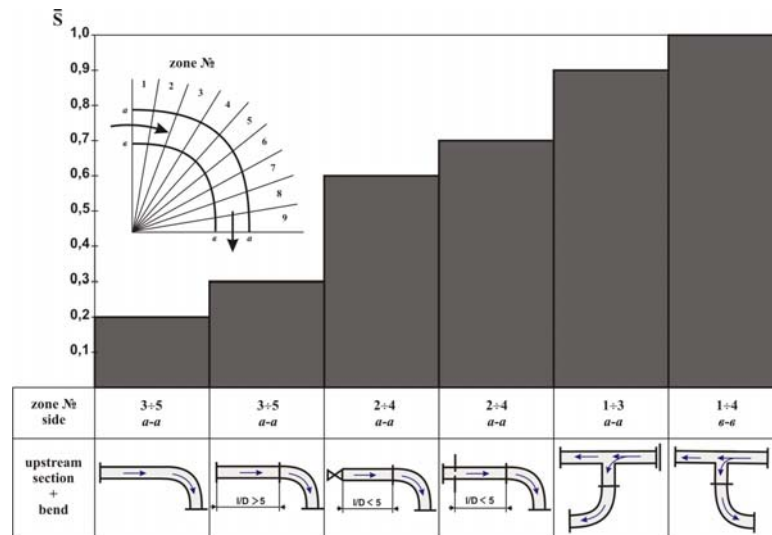


Figure 21 Effect of upstream section upon location of susceptibility zones (a) and local thinning rate (\bar{S}).

According to the Russian experience [57], mathematical modelling of local FAC processes by RAMEK allows to resolve urgent up-to-date problems (Figure 22):

- determination of maximum LFAC zones position in NPP pipelines and power equipment elements;
- ensuring safe allowable rate of FAC by way of elements design and operational conditions optimization;
- design of power equipment groups and pipelines units with equal operational life, both at engineering, operating and overhaul-period renewal stages.

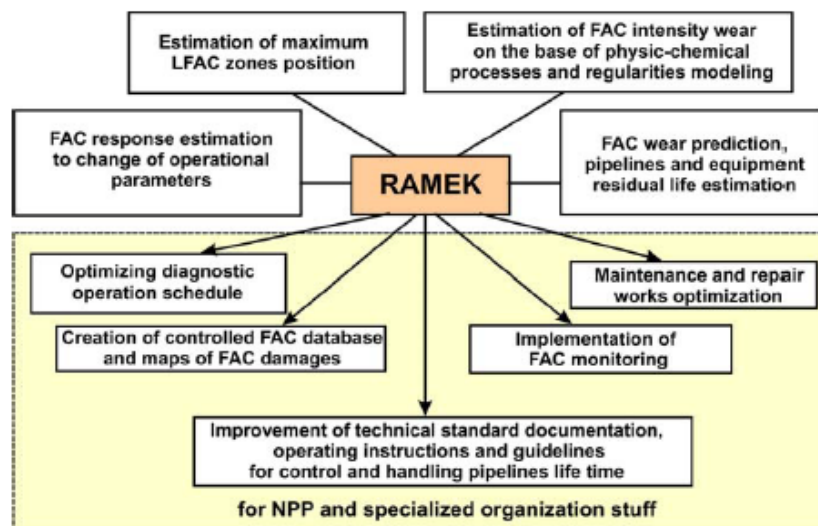


Figure 22 RAMEK as a basis of a comprehensive programme for NPP secondary circuit safe operation.

It is worth noting that in Russia, another series of codes has been developed and validated during the 1990s and early 21st century – the so-called ECI-01 to ECI-04, and also ECI-DS code [58-62] that have been certified for official use in all types of WWER plants (WWER-440 and WWER-1000) for both single-phase and dual-phase flows. Although no detailed description of these codes has been found in the open literature, a scheme of the FAC phenomenon that has served as a base for the codes is shown in Figure 23.

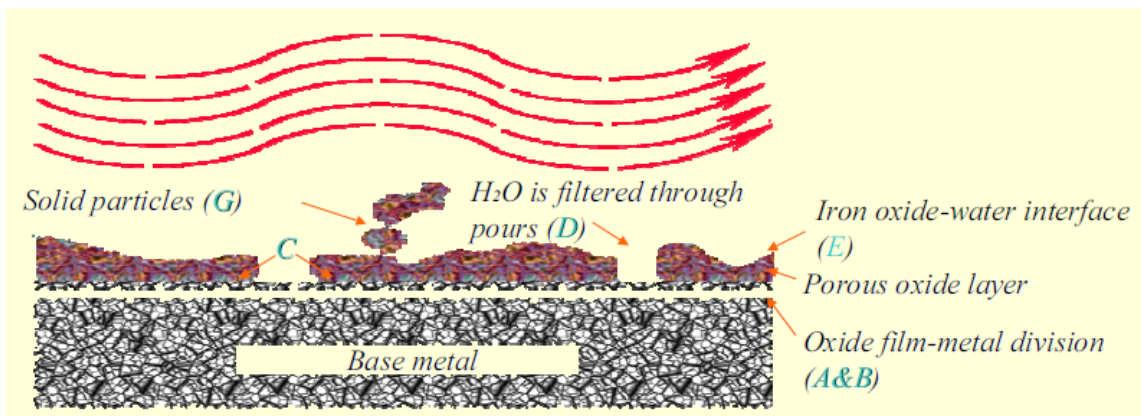


Figure 23 Scheme of the processes occurring during FAC according to the EK1 model [60]: A. Iron interaction with water and oxygen, B. Generation of magnetite according to the Schikorr reaction, C. Corrosion products generated during A&B reactions; D. Corrosion products dissolution in oxide layer pores; E. Corrosion products dissolution at the film/coolant interface; F. Coolant carries dissolved corrosion products away via mass transfer; G. the protective layer is washed out by the flow.

According to the authors [60], influence of the following factors is taken into account in the EK1 model:

- water chemistry indicators (type of amine applied, water pH, oxygen content in water);
- parameters of mode (water velocity and temperature);
- content of chemical elements in pipeline metal (chromium, molybdenum and copper)
- pipeline geometry (inner diameter, wall thickness, Keller factor)
- duration of operation (start and finish of pipeline operation).
- steam wetness (for ECI-DS software)

An example of the calculational results using ECI-01 software is presented in Figure 24.

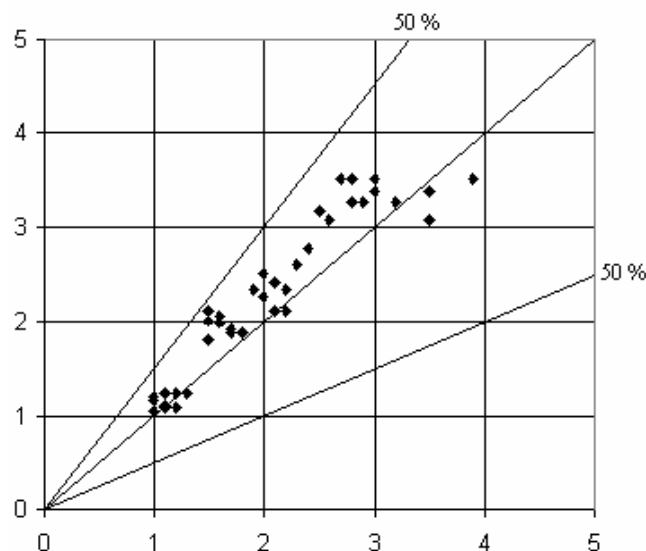


Figure 24 Comparison of calculation results by ECI-01 software (ordinate, in mm) with measurement data of wall thinning in feedwater pipelines (abscissa, mm) [61].

An important factor that appears to be taken into account in this software is the influence of the thickness of corrosion products accumulated on the internal surface of pipelines – the thicker the deposits are, the lower the rate of erosion-corrosion wear is [58]. However, the exact way by which this factor has been included has not been described in any detail to allow for a critical assessment of its importance to the predictive abilities of the software tool.

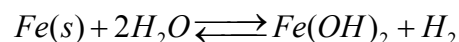
6 Discussion

6.1 Modelling of the corrosion process and the influence of the oxide layer

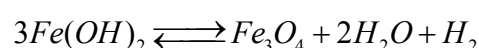
Even if most of the proposed quantitative approaches to flow-accelerated corrosion recognize the effect of the surface oxide layer on the wall thinning rate, the modelling of the growth and dissolution of the oxide film on carbon steel undergoing FAC is at the level of the 60s and 70s, mostly based on the works of Castle and Masterson [63], Bignold et al. [64] and Berge and Saint-Paul [65]. However, remarkable progress in the modelling of oxide films growth and restructuring on construction materials in high-temperature water has been achieved in the last 20 years, as summarized in recent reviews on the topic [66,67]. In the following, two important aspects of the influence of the oxide film on the reaction of divalent iron release as an integral part of the FAC phenomenon are considered – the thermodynamic aspect (i.e. the effect of different factors on oxide film nature and solubility) and the kinetics (i.e. the rate of dissolution of the oxide and rate of transfer of iron through the oxide into the water, respectively).

6.1.1 Thermodynamic aspect (oxide solubility)

On a carbon steel material, almost exclusively pure iron compounds are formed during the corrosion process in water. At lower temperatures, hydrolysed iron compounds as $\text{FeO}(\text{OH}) \cdot n\text{H}_2\text{O}$ (of Fe(III)) are formed at oxidising conditions and $\text{Fe}(\text{OH})_2 \cdot n\text{H}_2\text{O}$ (of Fe(II)) in reducing conditions [68]. The cathodic corrosion reaction in reducing conditions is hydrogen evolution from the surrounding water, and the net corrosion reaction can be written as



$\text{Fe}(\text{OH})_2 \cdot n\text{H}_2\text{O}$ will be transformed to magnetite relatively fast at LWR operating temperatures and reducing conditions according to the Schikorr reaction



The magnetite formation will release hydrogen gas, which in itself may produce local chemistries in constrained or low flow conditions [69]. The local conditions may affect the subsequent corrosion process in such locations but not so likely in high flow conditions as the hydrogen concentration would be rather insignificant. In oxidising conditions, hematite ($\alpha\text{-Fe}_2\text{O}_3$) and maghemite ($\gamma\text{-Fe}_2\text{O}_3$) are formed.

Maghemite has a spinel structure, forming large crystals acting as part of a protective oxide layer. The generally very microcrystalline hematite formed alternatively or additionally is not protecting against further corrosion but will act as an iron source for outer layer corrosion release and restructuring through reactions between the formed products and water.

The important processes for iron release involve the reverse reactions, as for the release (i.e. dissolution) of magnetite:



The dissolved iron is hence produced in the form of $Fe(OH)_2$. This compound will have a number of species of the form $Fe(OH)_n$, where n is 0 to 4 depending on temperature and pH. The total concentration of iron in this local system will, however, be governed by reaction (55) if this is the only source of iron, as shown by

$$[Fe^{2+}]_{tot} = K_{s,magnetite} \{Fe_3O_4(s)\}^{\frac{1}{3}} \{H_2O\}^{\frac{2}{3}} \{H_2\}^{\frac{1}{3}} \quad (56)$$

where $K_{s,magnetite}$ is the solubility constant of magnetite. The water activity is virtually unity, and the same is true for a pure magnetite phase. The iron solubility is hence given by the following expression

$$[Fe^{2+}]_{tot} = K_{s,magnetite} \{H_2\}^{\frac{1}{3}} \quad (57)$$

Expression (57) implies that the dependence of the hydrogen activity (fugacity) on magnetite solubility is not strong. This means that small hydrogen variations will in practice not affect the recorded or modelled iron solubility. Far more important is the redox potential at the oxide/water interface. In addition, pH and temperature will affect the exact form in which the dissolved iron is found. The reason is the amphoteric behaviour of the iron hydroxide, i.e. its ability to participate in acid-base equilibria. The iron speciation is given by equilibria of the type

$$K_1 = \frac{[Fe(OH)_2][H^+]}{[Fe(OH)^+]} \quad K_2 = \frac{[Fe(OH)_2][H^+]^2}{[Fe^{2+}]}$$

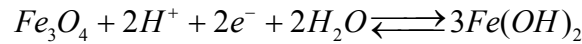
The total concentration of iron, $[Fe^{2+}]_{tot}$, is hence expressed as

$$[Fe^{2+}]_{tot} = [Fe(OH)_4^{2-}] + [Fe(OH)_3^-] + [Fe(OH)_2] + [Fe(OH)^+] + [Fe^{2+}]$$

This expression can be expanded to

$$[Fe^{2+}]_{tot} = [Fe(OH)_2] \left\{ \frac{K_w}{[H^+]^2 K_1} + \frac{K_w}{[H^+] K_2} + 1 + \frac{[H^+]}{K_1} + \frac{[H^+]^2}{K_2} \right\} \quad (58)$$

It is obvious that the speciation of iron is very strongly pH dependent. There is a pH at each temperature at which the expression within parentheses has a minimum. This is the pH at which thermodynamics imply that the least corrosion release would occur. Although also kinetics, i.e. the dissolution rate, has to be taken into account, equation (58) suggests that the (local) pH value is very important for the iron release from an iron (magnetite) containing oxide film. If (55) is written in a different form



it becomes clear that, at a certain pH, i.e. constant $[H^+]$, an “electronic scale” equalling a redox potential scale could be used to describe the behaviour according to thermodynamics at varying conditions. An interesting feature of this approach in the current context is that the electrochemical scale used in an LWR is the known, calculated [70,71], or accurately measured ECP in each location. This local property is much easier to assess than a well defined local hydrogen pressure in a system with presence of some oxidants. Even in PWRs and WWERs the ECP approach is the more generally applicable approach, since some oxidising species are present locally also in such plants, drastically changing the local ECP [70]. On the basis of this correlation, Bignold [72] derived an expression for the magnetite solubility on the ECP scale with $S_{magn, std}$ being the magnetite solubility at 1 bar hydrogen partial pressure in mol/l, and E the redox potential

$$[Fe^{2+}]_{tot} = S_{magn, std} [H^+]^{\left(\frac{2}{3}\right)} e^{\left(\frac{-2FE}{3RT}\right)}$$

This expression is illustrated in some examples of thermodynamic calculations for iron solubility (Figure 25). The reason for the occasional breaks in the slopes in the Figure is the formation of additional solid phases or new important species in the aqueous phase. Although kinetics has not yet been considered, it seems rather obvious that reducing conditions, which correspond typically to -500 to -700 mV vs. SHE in a PWR will result in a significantly higher iron solubility than oxidising conditions. Figure 25 also shows that the iron solubility increases with decreasing temperature, an example of so called retrograde solubility.

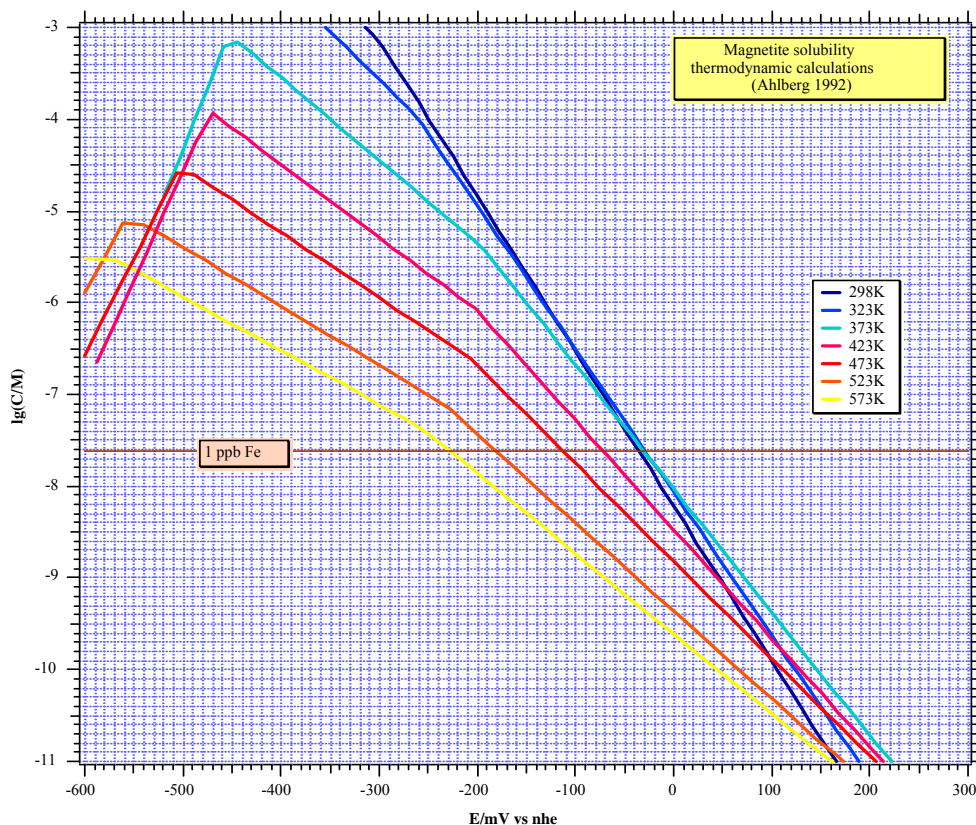


Figure 25 Iron solubility as a function of the potential at neutral pH, at varying temperatures, from thermodynamic calculations [67].

6.1.2 Kinetic aspect (growth and dissolution rates of the oxide)

A situation that cannot be quantitatively described by thermodynamic expressions is expected for oxides in LWR environments. This is due to the impact of limited reaction rates for one or several of the involved reactions. Both when it relates to interpreting or using laboratory and in-plant data, it is hence important to assess the impact of such a non-equilibrium situation. The reaction rate limitation could be either due to a limited mass transport rate or the dissolution kinetics that is limited. Since the slowest step is limiting the rate of the overall reaction, the corrosion rate, R , is given by

$$\frac{1}{R} = \frac{1}{R_{\text{masstransport}}} + \frac{1}{R_{\text{kinetics}}} = \frac{1}{R_{\text{mt}}} + \frac{1}{R_k}$$

Other steps than the steps at the water-oxide interface could be rate limiting, but any such step would also be rate limiting for the dissolution process. In very low flow systems, mass transport could be limiting. On the contrary, in cases where the flow rate is above more than some 10 m/s at LWR conditions, the mass transport rate in the water interface is important in order to describe and quantify FAC. For all other cases, it is adequate to state that

$$R = R_k$$

The temperature dependence of the release rate is given by the activation energy. In an early work, Potter and Mann [73] report the activation energy for magnetite dissolution (in carbon steel corrosion) to be $63 \pm 8 \text{ kJ mol}^{-1}$. This value is apparently widely different to the values reported by Robertson [74] for the corrosion rate for steel, i.e. 120 kJ mol^{-1} for solid phase diffusion of water molecules in the oxide film, which he concludes is the real rate limiting step, and $15\text{--}20 \text{ kJ mol}^{-1}$ for diffusion in the water filled pores in the magnetite film. Robertson's definition of the rate constant, designated, k_p , with the cited activation energy is, however, given as

$$x^2 = k_p t$$

with x being the oxide thickness and t the time. It is inferred that the rate constant defined to be linearly dependent on the oxide thickness squared, which seems natural if we consider oxide growth and corrosion release. The exponential Arrhenius relationship for the activation energy of oxide growth will be $60 \text{ kJ}\cdot\text{mol}^{-1}$ if we use Robertson's value of 120 kJ mol^{-1} for the diffusion reaction. The similarity between the values for magnetite dissolution by Potter and Mann, and Robertson, respectively, is rather striking. A very pronounced increase in magnetite dissolution rate with temperature is hence expected which would partly compensate the simultaneous decrease of iron solubility with temperature.

The duplex nature of the Fe_3O_4 film formed on carbon steel exposed to high-temperature ($150\text{--}300 \text{ }^\circ\text{C}$), de-oxygenated neutral and alkaline aqueous solutions is widely supported by experimental evidence [74]. The boundary between the layers has been found to lie at the position of the original metal surface, which indicates that the inner layer grows at the metal/oxide interface and that the outer layer grows at the oxide/solution interface. The inner layer consists of fine-

grained oxide because it grows in a confined space, while the outer layer consists of loosely packed, larger grains, because it grows without volume constraint. De Bakker et al. [75] found out that low temperature and low pressure in simulated pressurised water reactor (PWR) coolant, which corresponds to reducing conditions, led to the formation of partially oxidised-and-substituted magnetite on carbon steel. This was stated to be associated with severe corrosion. At high temperature and high pressure, small-particle partially oxidised-and-substituted magnetite with less severe corrosion problems was detected.

Summarizing, it can be stated that at least two parallel reactions proceed during the growth and dissolution of oxide films on carbon steel in high-temperature water (150-300 °C). The first reaction is the growth of an inner oxide layer via (most probably solid-state or easy path/shortcut) transport of oxygen from the water into the oxide, balanced by dissolution of this oxide at its interface with the water (with generation of soluble iron species) to maintain a steady state thickness. The second reaction is oxidation of iron at the metal/film interface followed by the transport of iron ions through the oxide and their dissolution in the water. The latter process can be followed by reprecipitation of oxide (at low flow rates) or transport of soluble iron species away from the interface into the boundary layer and further into the bulk solution (at high flow rates, relevant for the FAC phenomenon). In analogy to what has been recently shown for carbon steel during hot-conditioning primary heat transport systems in heavy-water reactors [76], the approach of the Point Defect Model and the Mixed-Conduction Model can successfully be used to represent the processes of growth and dissolution of oxides on such a material. Using this approach, it can be stated that at the steel / compact layer interface, one lattice-conservative reaction and one lattice-nonconservative reaction take place

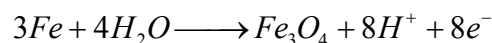


The transport of matter and charge through the inner compact film formed in the high-temperature electrolyte is assumed to be governed by the low-field approximation of the equations of Fromhold and Cook. In other words, solid-state transport via e.g. grain boundaries or other short circuit paths in the oxide is limiting the transfer rate at variance to the approaches used in the present FAC codes, in which it is assumed that water reaches the metal/film interface.

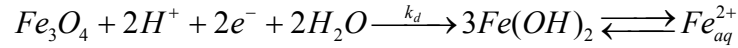
At the inner layer / electrolyte interface, the following lattice-conservative reactions proceed:



The sum of the reactions involving oxygen vacancies results in the growth of the inner magnetite layer on the steel surface



At steady state, the rate of the non-conservative reaction at the inner interface has to be balanced by the rate of dissolution of the compact layer e.g. by a reaction inverse to the Schikorr reaction



On the other hand, the sum of the reactions involving cation vacancies would lead to iron transfer from the metal through the oxide into the water flow. Obviously, as both reactions at the film/solution interface generate soluble divalent iron as their product, their kinetics could influence profoundly the rate of release of iron from carbon steel regardless of the flow rate and especially so in conditions that favour FAC, during which no secondary deposited layer is expected to be formed or if formed, it would not be a significant impediment to the dissolution process.

It can be concluded that a much needed refinement of the predictive ability of the models and associated software tools of FAC management would be an update and improvement of the submodel of oxide growth and dissolution. This can be done by incorporation of the already developed quantitative models for oxides on carbon and stainless steels in primary coolant conditions [76,77] into the respective software codes. This in turn would benefit from additional electrochemical and surface analytical characterisation of the oxides formed in FAC conditions in order to calibrate and validate the aforementioned models for these specific cases.

6.2 Hydrodynamics, mechanical effects, and boundary layer thickness

The correlation between hydrodynamical and mechanical parameters, such as the flow velocity and wall shear stress, in most of the proposed models and the associated codes is founded on the premise that FAC of carbon steel is mass-transfer controlled [28]. This, as detailed already above, is based on the postulate that there are two processes in series – the corrosion at the metal-oxide interface creating the oxide film there by half the iron that enters solution precipitating as magnetite (the rest diffuses through the film and is lost to the bulk coolant), followed by the dissolution of the film at the oxide-coolant interface by coolant undersaturated in dissolved iron.

Basically, mass transfer is described as convective diffusion. As the name suggests, this consists of convection in the bulk of the solution and diffusion in the immediate vicinity of the surface. Convective diffusion is expressed mathematically by a differential equation that includes Fick's first law and a convection term

$$J_i = D_i \text{grad} c_i + u c_i \quad (61)$$

where J_i is the molar flux of component i , D_i its diffusion coefficient, c_i the concentration of that component and u the flow velocity. In this equation, the fact that the dissolved iron is in ionic form (i.e. is a charged species) is not taken into account, which is certainly a drawback bearing in mind that the electrolyte is dilute and unsupported. The velocity field is expressed by the Navier-Stokes equations, which can be solved analytically only for a few simple geometries such

as the rotating disc. For turbulent flows and complex geometries, combinations of non-dimensional groups, known as mass transport correlations, can successfully be used:

$$Sh = aSc^b Re^c \quad (62)$$

where the Sherwood number Sh is the ratio of the total mass transport to mass transport controlled by molecular diffusion, the Reynolds number is the ratio of inertia force to friction force, and the Schmidt number is the ratio of momentum transport to mass transport via molecular diffusion. The practical significance of these correlations lies in the fact that Sh can be converted into corrosion rate, and Re is a function of the flow rate.

Correlations for mass transfer usually relate the dimensionless quantities Sherwood Number (Sh) and Reynolds Number (Re) to link the mass transfer to the flow characteristics. For constant physical properties of the system, this leads to an expression for FAC rate R of the type

$$Rd = ARe^p \quad (63)$$

where d is pipe diameter and A and p are constants. For many applications, the Re exponent p falls between 0.6 and 0.9 [52], whereas systematic Japanese-Canadian FAC experiments [28] have shown consistently higher exponents of 1.2-1.3.

An alternative approach has considered the Reynolds analogy of transport parameters in turbulent flow. The Stanton number for mass transfer ($Sh/Re/Sc$, where Sh is the Sherwood number and Sc is the Schmidt number) is equated to the friction factor ($\tau/(\rho \cdot u^2)$, where τ is the fluid shear stress and ρ is the fluid density. If the constant property terms are neglected and it is again assumed that corrosion rate is proportional to the mass transfer coefficient (i.e. that FAC process is mass-transport controlled), then proportionality between the corrosion rate R and the fluid shear stress is obtained

$$Ru = B\tau \quad (64)$$

Equation (64) apparently holds for FAC under these conditions of neutral chemistry, when magnetite solubility is high and corrosion is rapid [28]. Additional data, however, suggest that the assumption of mass-transfer control remains doubtful for high-pH chemistry, when magnetite solubility is comparatively low (about 14 ppb at 140°C under ammoniated conditions at pH_{25°C} of 9.2, in comparison with about 119 ppb under neutral conditions [78]). Thus more complex relationships are most probably needed to express the rate of FAC at higher pH values, including mixed surface reaction-convective mass transfer approaches combined with numerical calculations of the thickness of the boundary layer in such cases.

In general terms, the role of fluid hydrodynamics in FAC of steel depends on its effect on the corrosion layer formed on the electrode surface. An increasing flow velocity and shear stress would make thinner, degrade or even remove completely the scale, increasing corrosion of the steel. During fluid impingement, the shearing effect in the lateral direction increases with the decreasing impact angle, enhancing the removal of the corrosion scale from the steel surface. Therefore, an oblique impact of fluid would generally result in a high corrosion rate of the steel.

7 Conclusions

Although it is arguable on the basis of the present literature survey that degradation due to the FAC is predictable and manageable, there are still concerns caused by uncertainties involved in the evaluation methodologies. Considering the complexity of the mechanistic process of the FAC involving fluid and structure interaction, chemical reaction, convective or mixed mass transfer, erosion processes, and so on, it cannot be assumed that methods developed to predict susceptible locations and to assess the rate of metal loss are infallible and, therefore, conservatism should not be compromised during inspection planning activities. In the procedure for developing acceptable minimum thickness criteria, it is generally considered conservative to apply an allowable stress methodology. However, there are still a number of sources of uncertainty in the process of engineering evaluation for structural integrity of degraded pipes, which could erode safety margins. The sources of uncertainties may exist in:

- (1) Flaw modeling. In-service inspection techniques may not be sufficiently sensitive to characterize detected flaws, introducing the possibility of un-conservative modeling results.
- (2) Load calculation and combination, particularly for dynamic excitation. Feeder pipes are coupled to each other by spacers and also supported by various types of restraints, resulting in very complex dynamic behavior. Calculating responses of this complex piping system may lead to un-conservative results.
- (3) Residual stress. Magnitude of residual stress remaining in components and its effect on the component integrity is difficult to quantify. In turn, the effect of these stresses on the kinetics of film growth and restructuring, as well as the kinetics of dissolution, could be an important parameter that has not been taken into account by the existing modelling approaches.
- (4) Degradation of material properties. It is generally known and also observed in many actual cases that material properties may deteriorate due to operating conditions, leading also to a transformation of the surface oxides and hence their kinetics of dissolution which is one of the governing factors of flow-accelerated corrosion.

8 Summary

Flow-Accelerated Corrosion (FAC) of carbon steel occurs due to the dissolution of the protective film that is formed on the surface and directly contacted with water. FAC is a practical threat to carbon steel piping within Nuclear Power Plant (NPP) steam cycle systems. Without a systematic pipe management program, rupture or leakage of piping or pipe components due to wall thickness reduction due to FAC is inevitable. Pipe management program consists of several technical items, such as performing FAC model analyses, prioritizing pipe components for inspection, obtaining reliable thickness data, calculating the wear and wear rate, and making decisions regarding replacement necessity or continuous service acceptability based on the remaining life of the component. In the present literature review, the main emphasis is put on the predictive modelling of FAC including fundamental approaches such as the model of Sanchez-Calder and that of Lu and Luo, commercially available FAC rate prediction codes such as EPRI CHECWORKS, EdF BRT CICERO, KWU/AREVA WATHEC/COMSY, Russian codes such as RAMEK and ECI, as well as complex management

programs including proposal and validation of FAC countermeasures using both laboratory and in-plant operational data (coupling analysis of corrosion and fluid dynamics, local flow approaches to two-phase flow accelerated corrosion, combinations between predictive modelling and monitoring etc.). The strengths and weaknesses of all the approaches are compared. In a Discussion section, the unresolved problems and issues related to both the corrosion mechanism itself and the proper definition of hydrodynamic and mechanical factors is outlined.

References

1. W.H. Ahmed, *Ann. Nucl. Energy* 37 (2010) 598-605.
2. A. C. F. Guimaraes, *Ann. Nucl. Energy* 30 (2003) 853-864.
3. B. Poulson, *Wear* 233-235 (1999) 497.
4. R.B. Dooley, W.K. Chexal, *Int.J. Pressure V. Piping* 77 (2000) 85.
5. Schmitt, G., Bakalli, M., 2008. *Mater. Corros.* 59 (2), 181.
6. H.X. Guo, B.T. Lu, J.L. Luo, *Electrochim. Acta* 51 (2005) 315.
7. H.X. Guo, B.T. Lu, J.L. Luo, *Electrochim. Acta* 51(2006) 5341.
8. F. Vermorel, M. Romand, M. Charbonnier, M. Bouchacourt, *J. Phys. IV* 10(2000) Pr10-313.
9. S. Nazradani, R.K. Nakka, D. Hopkins, J. Stevens, *Int. J. Pressure V. Piping* 86 (2009) 845.
10. M.H. Koike, *J. Nucl. Mater.* 342(2005) 125.
11. M.H. Koike, *Corros. Sci.* 48 (2006) 617.
12. L.E.Sanchez-Caldera, P.Griffith, E.Rabinowicz, *Trans. ASME* 110 (1988) 180–184.
13. B.T. Lu, J.L. Luo, *J. Phys. Chem. B* 110(9) (2006) 4217.
14. W.Kastner, M.Erve, N.Henzel and B.Stellwag, *Nucl.Eng. Des.*119 (1990) 431-438.
15. A. Zander, H. Nopper, R. Roessner, Transactions of SMiRT 19, Toronto, 2007, Paper # D02/4, 8 p.
16. H. Nopper, A. Zander, Proc. FAC 2008, Lyon, France, 2008.
17. F.N.Remy, M.Bouchacourt, *Nucl.Eng. Des.* 133 (1992) 23-30.
18. D. Cubiciotti, *J. Nucl. Mater.* 152 (1988) 259.
19. E.Ardillon, B.Villain, M.Bouchacourt, Probabilistic Analysis of Flow-accelerated Corrosion in French PWR: The Probabilistic Module of BRT-CICERO Version 2.
20. T. Knook, M.Persoz, S.Trevin, S.Friol, M.-P. Moutrille, L.Dejoux, *E-Journal of Advanced Maintenance* 2 (2010/2011) 1-13.
21. S. Trevin, M. Perzol, I. Chapuis, FAC 2008 International Conference, March 18th to 20th, 2008 – Lyon (France), 1-11.
22. S. Uchida, M. Naitoh, Y. Uehara, H. Okada, S. Koshizuka, D.H. Lister, *ECS Transactions* 11(27)(2008)13.
23. M. Naitoh, S. Uchida, S. Koshizuka, H. Ninokata, N. Hiranuma, K. Dosaki, K. Nishida, M. Akiyama, H. Saitoh, *J. Nucl. Sci. Technol.* 45(11)(2008)1116.
24. S. Uchida, M. Naitoh, Y. Uehara, H. Okada, N. Hiranuma, W. Sugino, S. Koshizuka, *J. Nucl. Sci. Technol.* 45(12)(2008)1275.
25. S. Uchida, M. Naitoh, Y. Uehara, H. Okada, N. Hiranuma, W. Sugino, S. Koshizuka, D.H. Lister, *J. Nucl. Sci. Technol.* 46(1)(2009)31.
26. S. Uchida, M. Naitoh, Y. Uehara, H. Okada, T. Ohira, H. Takiguchi, W. Sugino, S. Koshizuka, *J. Nucl. Sci. Technol.* 47(2)(2010)184.

27. T. Satoh, Y. Shao, W.G. Cook, D.H. Lister, S. Uchida, *Corrosion* 63(8)(2007)771.
28. D.H. Lister, L. Liu, A. Feicht, M. Khatibi, W. Cook, K. Fujiwara, E. Kadoi, T. Ohira, H. Takiguchi, S. Uchida, Proc. XV Int. Conf. Properties of Water and Steam, Berlin, 2008.
29. S. Uchida, M. Naitoh, Y. Uehara, H. Okada, S. Koshizuka, D.H. Lister, Proc. FAC 2008, Lyon, France, 2008.
30. K. Ishida, Y. Wada, M. Tachibana, M. Aizawa, M. Fuse, E. Kadoi, *J. Nucl. Sci. Technol.* 43(1)(2006) 65.
31. K.-T. Ma, Y.-M. Ferng, Y.-P. Ma, *Nucl. Technol.* 123(1)(1998)90.
32. Y.-M. Ferng, Y.-P. Ma, K.-T. Ma, N.-M. Chung, *Corrosion* 55(4)(1999)332.
33. Y.-M. Ferng, Y.-P. Ma, K.-T. Ma, N.-M. Chung, *Nucl. Technol.* 126(3)(1999)319.
34. Y.M. Ferng, C.T. Hung, *Energy Conv. Management* 49 (2008) 1182.
35. Y.-M. Ferng, *Ann. Nucl. Energy* 35(2008) 304.
36. S.V. Patankar, D.B. Spalding, *Int. J. Heat Transfer* 15 (1972) 1787.
37. A. D. Gosman, P. J. K. Ideriah, "TEACH-2E: A General Computer Program for Two-Dimensional, Turbulent, Recirculating Flow," Department of Mechanical Engineering, Imperial College, 1976.
38. CHAM, "The PHOENICS Beginner's Guide," CHAM0 TR100, Concentration, Heat and Momentum Limited, 1991.
39. "CDFS-FLOW3D Release 3.3: User Manual," Computational Fluid Dynamics Services, 1994.
40. N.Y. Lee, S.G. Lee, K.H. Ryu, I. S. Hwang, *Nucl. Eng. Des.* 237(2007) 761.
41. K.H. Ryu, I. S. Hwang, N.Y. Lee, Y.J. Oh, J.H. Kim, J.H. Park, C.H. Sohn, *Nucl. Eng. Des.* 238(2008)3283.
42. K.H. Ryu, T.H. Lee, J.Hak Kim, I. S. Hwang, N.Y. Lee, J.Hyun Kim, J.H. Park, C.H. Sohn, *Nucl. Eng. Des.* 240(2010) 468.
43. R.G. Keck, P. Griffith, *ASME J. Eng. Gas Turb. Power* 112(1990)555.
44. W. Von Kastner, K. Riedle, *VGB Kraftwerkstechnik* 66 (1986) 1171.
45. F. Sweeton, C. Baes, *J. Chem. Thermodynamics* 2 (1970) 479.
46. A. Roine, Outokumpu HSC Chemistry for Windows: Chemical Reaction and Equilibrium software with extensive thermochemical database, User's Guide, Ver.4.0, 1999.
47. P. Goyal, R. Rastogi, V. Verma, V. Bhasin, R. K. Singh, K. K. Vaze, A. K. Ghosh, Proc. FAC 2008, Lyon, France, 2008.
48. WATHEC/DASY. Flow-accelerated Corrosion Software. Siemens/KWU, 1991.
49. J.A. Wharton, R.J.K. Wood, *Wear* 256(2004)525.
50. V. Kain, S. Roychowdury, T. Mathew, A. Bhandakkar, *J. Nucl. Mater.* 383 (2008) 86.
51. X.-X. Yuan, M.D. Pandey, G.A. Bickel, *Nucl. Eng. Des.* 238(2008)16.
52. F.P. Berger, K.-F.F.-L. Hau, *Int. J. Heat Mass Transfer* 20 (1977) 1185.
53. G.V. Tomarov, *J. Thermal Eng.*, 7 (1989) 33.
54. G.V. Tomarov, *J. Thermal Eng.*, 48(9) (2001) 761.
55. G.V. Tomarov, A.A. Shipkov, *J. Thermal Eng.*, 49(7) (2002) 530.
56. G.V. Tomarov, A.A. Shipkov, M. Kasimovsky, *Transactions of SmiRT 19*, Toronto, 2007, paper B06/3.
57. G.V. Tomarov, A.A. Shipkov, Proc. FAC 2008, Lyon, France, 2008.
58. V.I. Baranenko, A.V. Kumov, Yu.A. Yanchenko, A.S. Prokopenko, *Thermal Eng.* 54 (2007) 981.
59. V. I. Baranenko, Yu.A. Yanchenko, *Thermal Eng.* 54 (2007) 348.

60. V. I. Baranenko, Yu.A. Yanchenko, in IAEA technical workshop on erosion-corrosion wear including flow accelerated corrosion (FAC) and environmentally assisted cracking (EAC) issues at nuclear plants, Moscow, 2009, paper No.11.
61. V. I. Baranenko, in IAEA technical workshop on erosion-corrosion wear including flow accelerated corrosion (FAC) and environmentally assisted cracking (EAC) issues at nuclear plants, Moscow, 2009, paper No.22.
62. M. Bakirov, in IAEA technical workshop on erosion-corrosion wear including flow accelerated corrosion (FAC) and environmentally assisted cracking (EAC) issues at nuclear plants, Moscow, 2009, paper No.6.
63. J.E. Castle, H.G. Masterson, *Corros. Sci.* 6 (1966) 93.
64. G.J. Bignold, R. Garnsey, G.M.W. Mann, *Corros. Sci.* 12 (1972) 325.
65. P. Berge, C. Ribon, P. Saint Paul, *Corrosion* 32 (1976) 223.
66. I. Betova, M. Bojinov, T. Laitinen, K. Mäkelä, T. Saario, STUK-ITO-TR 150, Finnish Nuclear Safety Authority, 1999, 78 p.
67. M. Bojinov, P. Kinnunen, K. Lundgren, G. Wikmark, VTT Report NO BTUO73-041285, 2004, 143 p.
68. C.F. Cheng, *Corrosion* 20 (1964)341.
69. M. Warzee, J. Hennaut, M. Maurice, C.Sonnen, J.Waty, Ph. Berge, *J. Electrochem. Soc.* 112 (1965) 670.
70. G. Wikmark, K.Lundgren, In Proc. 8th Intl. Conf. Water Chem. Nucl. Power Plants, BNES, Bournemouth, UK; 22-26 Oct 2000, Vol. 1, 164-169, 2000
71. K. Lundgren, H. Wijkström, G. Wikmark, Proc. Int'l Conf. Water Chem Nucl.Reactor Systems, San Francisco, October 11-14, 2004.
72. G.J. Bignold, C.H. de Whalley, K. Garbett, I.S. Woolsey, In Proc. BNES Conf. Water Chem. Nucl. Reactor Syst. 3, 1 (1983)219–226.
73. E.C. Potter, G.M.W. Mann, In Proc. 2nd Int'l Cong. Metallic Corr., NACE, 1966,872–879.
74. J. Robertson, *Corr. Sci.* 29 (1989)1275.
75. P.M.A. de Bakker, M. Verwerft, M. Wéber, E. De Grave, in Water chemistry of nuclear reactor systems 7. London: British Nuclear Energy Society, 1996, 100-102.
76. M. Bojinov, K. Gaonkar, S. Ghosh, V. Kain, K. Kumar, T. Saario, *Corros. Sci.* 51 (2009) 1146.
77. M. Bojinov, P. Kinnunen, K. Lundgren, G. Wikmark, *J. Electrochem. Soc.* 152 (2005) B250.
78. P.R.Tremaine, J.C. LeBlanc, *J. Solution Chem.* 9 (1980)415.